Study on properties and factors of high concentration ozone in summertime in Kanto region of Japan

(夏季の関東地方における高濃度オゾンの特徴と要因に関する研究)

December　2014

Yusuke Kiriyama

(桐山　悠祐)

Abstract

In recent years, ground-level ozone concentrations tend to increase in summertime in Kanto. Emissions of ozone precursors (nitrogen oxides and volatile organic compounds) have been reduced due to various emission controls, and, as a result, ambient concentrations of the precursors have been decreasing. However it is still not clarified that the emission reductions are effective on variations of ozone concentrations. In summertime, ozone concentrations often become higher in inland Kanto (Northern Saitama, Gunma and Tochigi) than in and around central Tokyo. It is well known that ozone and its precursors are transported by sea breezes from Tokyo Bay to inland Kanto. However high concentration ozone is also observed in the morning before sea breezes reach inland Kanto. In this study, numerical simulations are conducted to 1) evaluate the effects of emissions reductions of the precursors on ozone concentrations in Kanto and 2) to find out the cause of morning high concentration of ozone in inland Kanto.

Through numerical simulations, it is shown that emission reductions of the precursors contribute to increases of daytime maximum ozone concentrations in highly urbanized areas along Tokyo Bay and to decreases by 2-3 ppb in the other area of Kanto. In case that emissions of nitrogen oxides are solely reduced, daytime maximum concentration ozone increased by 1-3 ppb in a wide area of Kanto. In case that emissions of volatile organic compounds are solely reduced, daytime maximum concentration of ozone decrease by 2-5 ppb in entire Kanto. The simulated results are analyzed for sensitivity of ozone concentrations to emission reductions of the precursors. From the results of ozone sensitive analysis for high concentration day, reductions of NOx emissions were effective for reduction ozone concentrations in inland Kanto. On the other hand, reductions of VOC emissons highly influenced to decreases of ozone concentrations in coastal area.

It is shown that ozone concentrations in inland Kanto are less influenced by the precursors emitted in the metropolitan area (southern Saitama, eastan Tokyo, eastern Kanagawa and western Chiba) than those emitted out of the area. Moreover, calculated results indicate that the morning increase of ozone concentrations in inland Kanto is influenced by downward transport of ozone that remains aloft during nighttime. The residual ozone is also contributed by the precursors emitted from out of the metropolitan areas.

Contents

1. Introduction

1.1 The problem of the high concentration ozone near the surface

A great deal of ozone (O_3) is distributed throughout the stratosphere, and the concept of the ozone layer is familiar to many people. This stratospheric ozone layer attenuates the ultraviolet (UV) rays contained in sunlight and shields humans and other organisms from their damaging effects, and is thus generally recognized as beneficial. However, O_3 is also distributed near ground level. Although its concentration near the surface is lower than in the stratosphere, it is nevertheless harmful to many organisms because it is a powerful oxidant (e.g. US Environmental Protection Agency, 2006; Nawahada et al., 2012; Wang et al., 2005).

High concentrations of O_3 were reported in Japan for the first time in the 1970's with high economic growth, and came to be known to the public as "photochemical smog" or "photochemical oxidants". The Japanese government has enacted various measures to control anthropogenic emissions and mitigation of O_3 air pollution (measures are listed in Table 1.1; for details, see Wakamatsu et al. 2013). For example, emissions of two types of O_3 precursors—nitrogen oxides (NOx; i.e. nitrogen monoxide (NO) and nitrogen dioxide (NO_2)) and volatile organic compounds (VOCs; also known variously as non-methane hydrocarbons (NMHCs) or non-methane volatile organic compounds (NMVOC) in other publications)—were regulated by amendments to air pollution control laws that targeted stationary emission sources. The government of Japan also controls vehicular emissions through legislation such as the Road Transport Vehicles Act (Amendment) for CO, NOx, and Hydrocarbons Emissions in 2000 and the Law Concerning Special Measures for Total Emission Reduction of NOx and Particulate Matter (PM) from Automobiles in Specified Areas (The Automobile NOx/PM Law) in 2001. The Automobile NOx/PM Law regulates the emissions of NOx and particulate matter from cargo trucks, buses, and diesel passenger vehicles that drive within the more heavily polluted prefectures in the Kanto, Tokai, and Kansai regions, which are some of Japan's major urbanized areas. Moreover, the prefectures of Tokyo, Saitama, Chiba, and Kanagawa in Kanto and Osaka and Hyogo in the Kansai region regulate the inflow of vehicles that fail to meet standards.

As seen from the above, a number of emission control laws have attempted to provide solutions to O_3 pollution. As a result, ambient concentrations of O_3 precursors have been decreasing in Japan, as shown in Figure 1.1 (Ministry of Environment, 2014). Nevertheless, daytime maximum O_3 have tended to increase nationwide (Ministry of the Environment, 2014). Moreover, attainment ratios for meeting the air quality standards for O_3 remain extremely low.

Table 1.1 Examples of emission control law (Wakamatsu et al., 2013).

The name of laws (short name)	Outline
The air pollution control law (1968)	The law defines the standard of emission for each chemical matter. Business operators is liable for compliance with the regulations
Total pollutant volume control on nitrogen oxides (1981)	Regulation for strong areas. The law regulates the emission not only from each plant but also in each area.
The automobile NOx・PM law (2001)	The law regulates the emissions of NOx and particulate matter from automobiles driven on major urbanized areas of Japan.
Amendment of the air pollution control law (for regulation of VOC emissions, 2006)	VOC emission regulation for the plants which emit VOC.

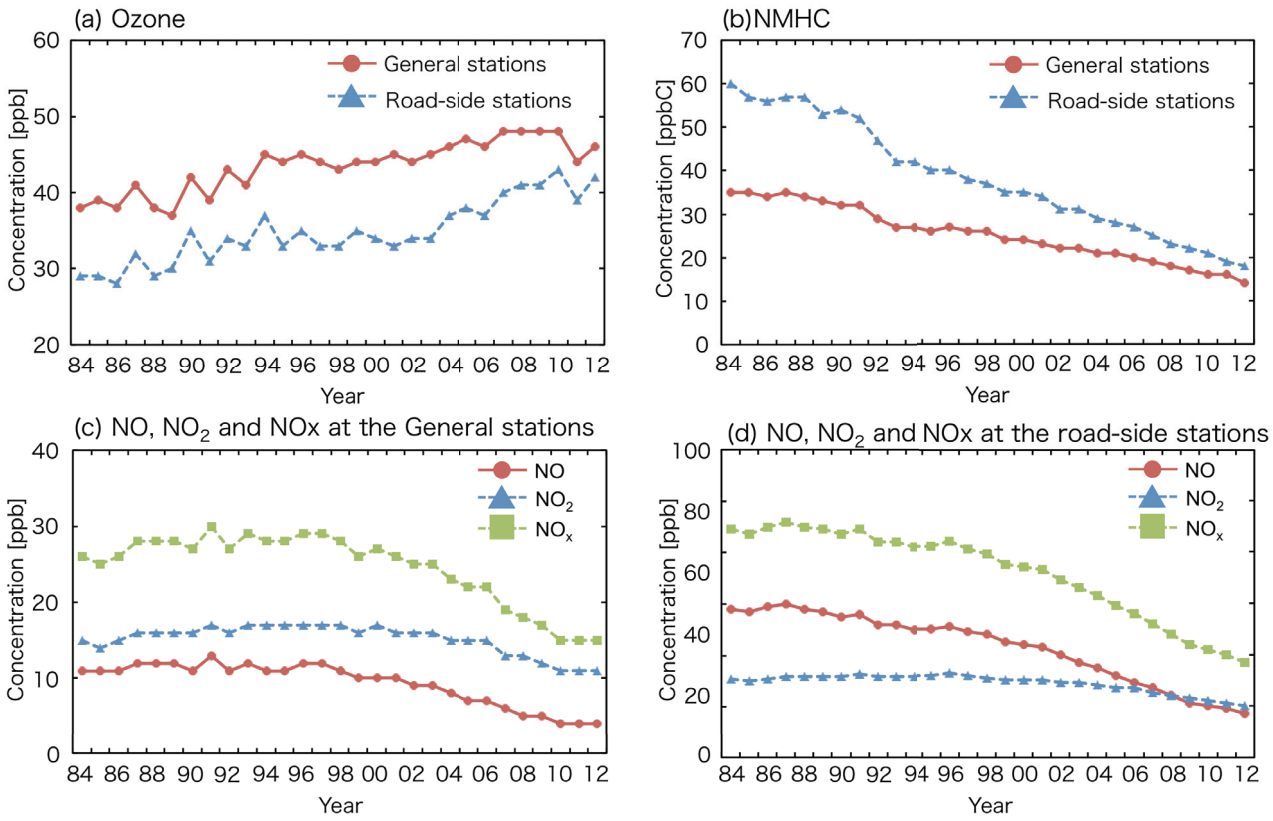

Fig. 1.1 Trends of annual average of O_3 and its precursors in Japan.

(a): O_3, (b): NMHC, (c): NO, NO_2 and NOx at the general stations and (d): NO, NO_2 and NOx at the road-side stations. The general stations have been placed to monitor a regon-wide atmospheric situation. The road-side stations have been placed to monitore a atmospheric pollution situation caused by automobile traffic. Original data of these figures were obtained from the Atmospheric Environmental Regional Observation System.

Therefore, improvement of O_3 air pollution is strongly desired.

1.2 Chemical reactions between O_3 and its precursors

Chemical reactions between O_3 and its precursors are very complex, and therefore, this section will go over core reactions.

O_3 production reactions from NOx are expressed as follows:

$$NO_2 + h\nu \rightarrow NO + O \quad (\nu < 424\text{nm}) \qquad \text{(R1)}$$

$$O + O_2 + M \rightarrow O_3 + M \qquad \text{(R2)}$$

$$\text{(net):} \quad NO_2 + h\nu \rightarrow O_3 + NO \text{ (in the presence of } O_2) \qquad \text{(R3)}$$

Here, M is a third body in the reactions, and represents any molecule that does not participate in the reaction such as N_2 or O_2. R1 is a photochemical reaction and therefore does not occur at night. In contrast, an O_3 loss reaction is expressed as follows:

$$NO + O_3 \rightarrow NO_2 + O_2 \qquad \text{(R4)}$$

Unlike reaction R1, this reaction is not photochemical and therefore can occur at any time. Moreover, O_3 is also produced through reactions involving hydrocarbons (described as RH in this section, where R represents an organic group), expressed as follows.

$$RH + OH \rightarrow RO_2 + H_2O \text{ (in the presence of } O_2) \qquad \text{(R5)}$$

$$RO_2 + NO \rightarrow RO + NO_2 \qquad \text{(R6)}$$

$$RO + O_2 \rightarrow R'CHO + HO_2 \qquad \text{(R7)}$$

$$HO_2 + NO \rightarrow OH + NO_2 \qquad \text{(R8)}$$

$$\text{(net):} \quad RH + 4O_2 \rightarrow R'CHO + 2O_3 + H_2O \text{ (with reaction R3)} \qquad \text{(R9)}$$

Here, RO_2 is an alkyl peroxy radical, and RO is an alkoxy radical. O_3 is then produced in reactions R6 and R8 (due to R3 following these reactions). The chain reaction from R5 to R8 will be terminated by losses of HOx (OH radicals and HO_2 radicals). The reactions in which the HOx radical is lost are mainly expressed as follows.

$$HO_2 + HO_2 \rightarrow H_2O_2 + O_2 \qquad \text{(R10)}$$

$$NO_2 + OH + M \rightarrow HNO_3 + M \qquad \text{(R11)}$$

R10 will occur under low NOx concentrations, and R11 will occur under high NOx concentration. O_3 production rate

(P_{O3}) in the chain reaction from R5 to R8 is expressed as follows.

$$P_{O3} = k_6[RO_2][NO] + k_8[HO_2][NO] \fallingdotseq 2k_8[HO_2][NO] \quad (1.1)$$

Here, k_a is the reaction rate constant for reaction (Ra) and [A] is the concentration of chemical species A. Each value of k_a is shown in Table 1.2. Approximation of the second and third terms is applicable in polluted air, and the chain reaction rapidly proceeds. The loss rate of HOx (L_{HOx}) due to reactions R10 and R11 will be expressed as follows.

$$L_{HOx} = 2k_{10}[HO_2]^2 + k_{11}[NO_2][OH][M] \quad (1.2)$$

Moreover, OH will be at a steady state in polluted air. Therefore, OH production (R8) and loss (R5) will be balanced. The concentration of OH will be expressed as follows.

$$k_5[RH][OH] = k_8[HO_2][NO]$$

$$\text{therefore} \quad [OH] = k_8[HO_2][NO] / k_5[RH] \quad (1.3)$$

When the NOx concentration is very low, Eq. 1.2 will be as follows.

$$L_{HOx} = 2k_{10}[HO_2]^2 \quad (1.2')$$

As a consequence, Eq. 1.1 will be changed by Eq. 1.2' as follows.

$$P_{O3} = 2k_8(L_{HOx}/2k_{10})^{1/2}[NO] \quad (1.4)$$

In this situation, NO concentration controls O_3 production, while RH concentration does not contribute to O_3 production. Therefore, reduction of NO (i.e. NOx) emissions can be effective for decreases of O_3 concentrations. Under high concentrations of NOx, Eq. 1.2 changes as follows.

$$L_{HOx} = k_{11}[NO_2][OH][M] \quad (1.2'')$$

The HO_2 concentration will be expressed as follows due to Eqs. 1.2'' and 1.3.

$$[HO_2] = k_5L_{HOx}[RH] / k_8k_{11}[NO_2][NO][M] \quad (1.5)$$

Therefore, Eq. 1.1 will be changed by Eq. 1.5 as follows.

$$P_{O3} = 2k_5L_{HOx}[RH] / k_{11}[NO_2][M] \quad (1.6)$$

In this situation, an increase or decrease of the RH concentration leads to an increase or decrease of the O_3 concentration, respectively. However, a decrease of the NO_2 concentration leads to an increase of O_3 concentration. Therefore, reductions of RH (i.e. VOCs) are effective for decrease of the O_3 consentration, but emissions reductions of NO_2 (i.e. NOx) are counterproductive. Figure 1.2 shows a relationship between emissions of NOx and VOC, and the O_3 concentration. If the atmosphere is in the situation as upside of bold line in Fig. 1.2, reductions of NOx emissions lead

to decrease of O_3 concentration. But reductions of VOC emissions do not make large changes on the O_3 concentration. Meanwhile, the atmosphere is in the situation as downside of bold line in Fig. 1.2, reductions of VOC emissions lead to decrease of O_3 concentration but reductions of NOx emissions increase the O_3 concentration. As shown in Eqs. 1.4 and 1.5 or Fig. 1.2, non-linear relationships exist between O_3 and its precursors (NOx and VOC). Given the nature of these chemical relationships, emission reduction controls will have different effects depending on the place they are implemented and the time.

Table 1.2 Summary of reaction rate constants (derived from Seinfeld and Pandis, 2006)

No.	Reaction	Reaction rate constants, k_a at 298 K [cm^3/molecule/sec]
(R1)	$NO_2 + h\nu \rightarrow NO + O$ (ν < 424nm)	0.015 [/sec]
(R2)	$O + O_2 + M \rightarrow O_3 + M$	6.0×10^{-34}
(R4)	$NO + O_3 \rightarrow NO_2 + O_2$	1.9×10^{-14}
(R5)	$RH + OH \rightarrow RO_2 + H_2O$ (in the presence of O_2)	26.3×10^{-12} a
(R6)	$RO_2 + NO \rightarrow RO + NO_2$	7.7×10^{-12} b
(R7)	$RO + O_2 \rightarrow R'CHO + HO_2$	1.9×10^{-15}
(R8)	$HO_2 + NO \rightarrow OH + NO_2$	8.1×10^{-12}
(R10)	$HO_2 + HO_2 \rightarrow H_2O_2 + O_2$	2.9×10^{-12}
(R11)	$NO_2 + OH + M \rightarrow HNO_3 + M$	2.5×10^{-11} c

a: at 1013 hPa. RH equals to Propene.

b: R equals to CH_3.

c: High pressure limit rate constant.

Low pressure limit rate constant is 2.0×10^{-30} [cm^6/$molecule^2$/sec]

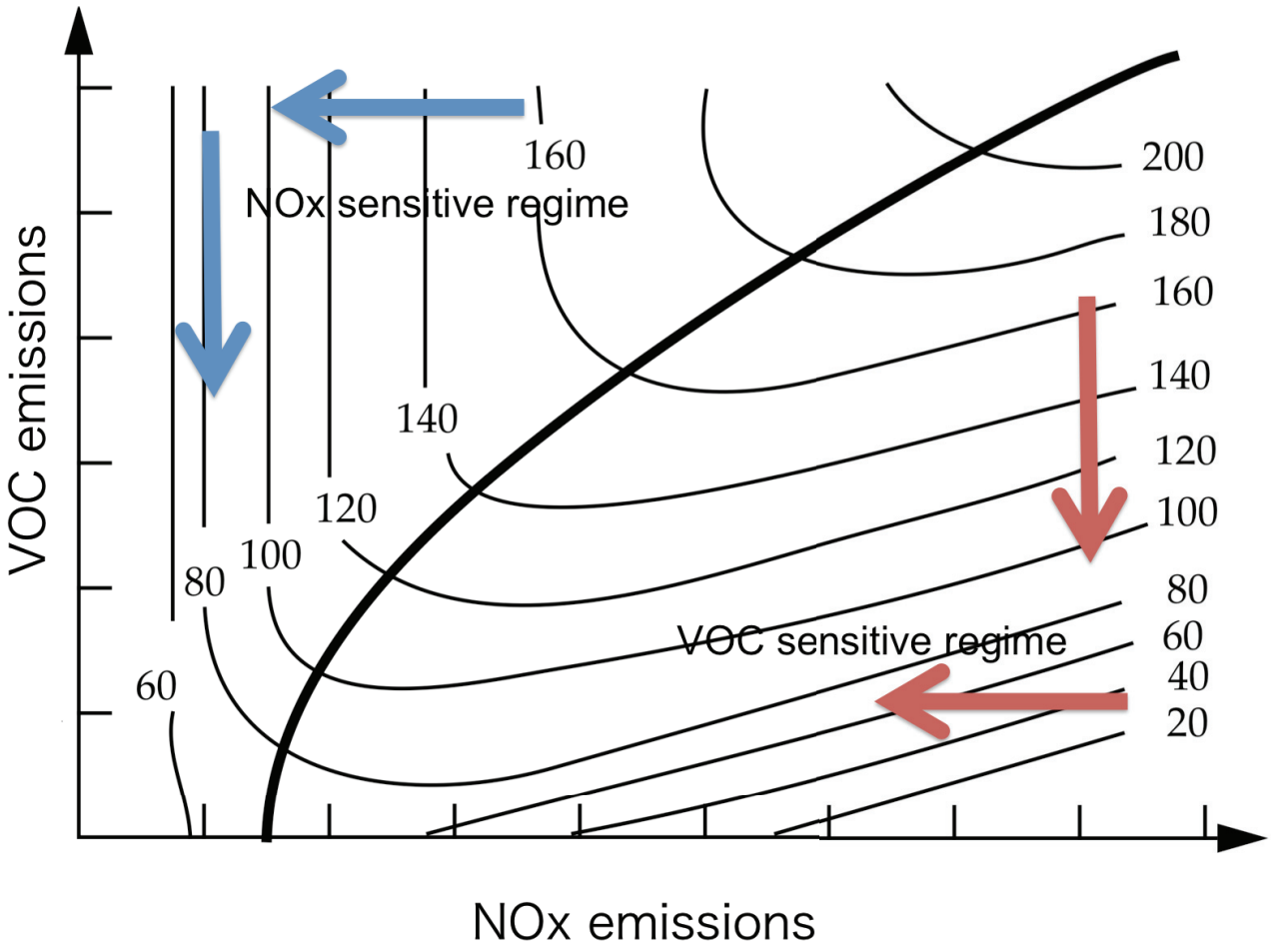

Fig. 1.2 Relationship between O_3 and its precursors, NOx and VOC (original figure was derived from Jacob, 1999). Isopleths indicate the maximum concentration of O_3 and numbers that were written on Isopleths indicate O_3 concentrations.

The bold line passes through extreme values. On the upside of the bold line, the O_3 concentration decreases with decreasing NOx emissions. While, decrease of VOC emissions do not makes large changes in the O_3 concentration. On the other hand, on the downside of the bold line, the O_3 concentration increases with decreasing NOx emissions. But reductions of VOC emissions is effective for the reduction of O_3 concentration.

1.3 Factors for the occurrence of high concentration ozone

As shown in Section 1.1, the surface O_3 concentration in Japan is still high. The main possible factors accounting for this occurrence are listed below.

1. Downward transport from the stratosphere (the O_3 layer) to the troposphere.
2. Transboundary transport of O_3 and its precursors from other industrial countries in East Asia.
3. Influences of domestic emissions of O_3 precursors.

Muramatsu (1980) showed that the first factor was most pronounced in spring. Nagashima et al. (2010) further showed, using a global chemical model, that the contribution of stratospheric O_3 to surface O_3 concentration is larger in spring than that in summer in East Asia. Transboundary air pollution came to public attention in January 2013, when the $PM_{2.5}$ concentration increased to extremely high levels in large cities in China. Transboundary transport of pollutants from industrial countries in East Asia are seen as important effects on O_3 concentration in Japan. However, these effects are diminished in summer, when an anticyclone develops in the Pacific Ocean near Japan bringing air masses from the ocean. Thus, the contribution of the polluted air masses from the East Asian continent is lowered in summer compared to in spring. Nagashima et al. (2010) also reported that the contribution of O_3 precursors from foreign countries to surface O_3 concentration in central Japan was about 80%. Of this contribution of O_3 precursors from foreign countries, China, Korea, and their adjacent sea accounts for about 30%. Conversely, in summer, the contribution of domestic sources is dominant to surface O_3 concentration in central Japan, accounting for about 40%. Pochanart et al. (2002) used observation results and backward trajectory analyses to demonstrate that remote islands in the Sea of Japan were influenced by polluted continental air masses. On the other hand, the Pacific Ocean side of Japan was mainly influenced by clean maritime air masses, and less influenced by transboundary air pollution in summer than other seasons. Reports from Ministry of Environment (2014) showed that O_3 concentrations remarkably increased in western Japan, especially in Kyushu, whereas the increase was moderate in eastern Japan. The effect of transboundary air pollution on the surface O_3 concentration is therefore greater in western Japan.

As mentioned above, O_3 precursors emitted from domestic sources might contribute to high concentrations of O_3 in Kanto. The population of this region is heavily concentrated in and around the 23 wards of the Tokyo Metropolitan Area, and many factories and power plants are situated around Tokyo Bay. Therefore, anthropogenic emissions from stationary and mobile emission sources contribute greatly in the large coastal urban areas, and less so in the more rural

parts of the Kanto region. As shown in Section 1.1, the concentration of O_3 precursors has gradually decreased year-by-year due to emission controls. The relationship between emission controls and variations in O_3 concentration has been examined in many studies. For example, Gégo et al. (2008) studied the effect of the decrease in NOx emissions from power plants in the eastern United States on variations of O_3 concentrations, using meteorological and chemical transport models. Their results indicated that 8-hour mean O_3 concentrations decreased, especially at high concentration ranges, in the eastern U.S. as a result of a decrease in NOx emissions. Moreover, Ministry of Environment (2012) showed that 7% to 20% decreases in O_3 concentrations were a consequence of a 30% reduction in VOC emissions from stationary sources. However, as many studies have pointed out, the effects of emission controls likely result in location- and time-based variations due to the non-linear dependence of the O_3 concentration on NOx and VOC emissions (as summarized in Section 1.2). Therefore, it is necessary to evaluate the effects of emission reductions on O_3 concentrations to consider more effective emission control measures and long-term improvement of the atmospheric environment.

Sea breezes, which occur according to the difference in specific heat between sea and land, play an important role in the cycle of pollutants in summer in Kanto. Wakamatsu et al. (1983) showed that sea breezes have a major impact on three-dimensional distributions of O_3. Moreover, sea breezes increase O_3 concentrations in the inland Kanto region by transporting pollutants from the coastal area. Kurita et al. (1985) showed that persistent sea breezes caused by thermal low could transport pollutants to the area far from industrial and populated areas. Many studies focusing on O_3 air pollution in Kanto indicated that high concentrations of O_3 moved from the large coastal urban area to the interior with the transport of O_3 precursors by sea breeze. However, Ministry of Education (1986) showed that the O_3 concentration in Kumagaya and Fukaya of Saitama Prefecture increased from about 20 and 10 ppb to about 70 and 80 ppb, respectively, in the morning before O_3 and its precursors driven by sea breezes arrived (the first peak) and O_3 concentrations increased again (the second peak) in the afternoon. Ministry of Education (1986) had considered that a possible cause of the first peak was production from O_3 precursors emitted in and around inland Kanto and that the second peak was caused by the transport of O_3 and its precursors by sea breezes. These two peaks of O_3 concentrations mean that O_3 concentrations remain high for a long period and, therefore, people are exposed to high concentration of O_3 for a long time. Kiriyama et al. (2012) found the similar diurnal patterns at the observation stations in Gunma Prefecture and showed that the entrainment of upper residual O_3 due to development of the mixed layer (or planetary

boundary layer) would contributed to the first peak. Niwano et al. (2007) showed that O_3 transported by the sea breeze remained in the upper air above inland Kanto. Despite these studies, however, the contribution of O_3 precursors and residual O_3 to the first peak of diurnal O_3 variation and upper residual O_3 in inland Kanto has not yet been evaluated in detail.

1.4 The purpose of this study

As shown in Sections 1.1 and 1.3, improvement of O_3 air pollution is not observed. Attainment ratios of the air quality standard for O_3 are still extremely low in spite of decreases in the concentration of O_3 precursors. Because of its harmful properties, a solution to the problem of O_3 air pollution is urgently required.

A compelling way to study air quality is through observation of meteorological parameters (e.g. temperature, relative humidity, wind direction, or wind speed) and concentrations of various pollutants in the atmosphere. Another powerful method is the use of numerical experiments with models that simulate the meteorological and atmospheric chemical processes. Ministry of Environment (2014) reported the trends and relationships of O_3 and its precursors by using statistically analyzed monitoring data and provided important insights for Japan's future emission control measures. However, it is difficult to obtain dense three-dimensional data over the long term and to comprehend and quantify the relationships between emission sources and high concentration of individual O_3. Numerical model simulations can be utilized in response to these problems. For example, calculation periods and resolutions that meet with the purpose of researchers can be set in numerical model simulations, which can also easily trace chemical reactions and the transport process. Moreover, numer3ical models can analyze the sensitivity of various atmospheric components as they relate to one another by perturbing parameters. These capabilities constitute major differences from standard observation methods. Nagashima et al. (2010) provides an example of a numerical model study that was able to uncover results that would have been difficult to detect by observation. Many other studies also used numerical models to attempt to uncover the source of O_3 air pollution over East asia and transboundary air pollution. Although, less model studies forcused on Kanto, especially evaluation of emission controls on Kanto than studies forcused on East asia.

The purpose of the present study is to clarify the cause of high concentrations of O_3 in the inland Kanto region and to evaluate the effect of emission controls in Japan on O_3 concentration in the region by using numerical models. As shown in section 1.3, it is considered that the influence of O_3 and its precursors from the foreign countries to the

high-concentration O_3 in Japan would be small in summer compared to in the other seasons. In this study, causes of the high concentration ozone resulted from domestic sources were analyzed. It is considered that Kanto in summertime is suitable as a subject of the present study, because the influence of transboundary air pollution on high concentration O_3 in summer is smaller than other sesons. Figure 1.3 shows annual and summertime averages of daytime maximum ozone concentrations. It is shown that daytime maximum ozone concentrations in Kanto also tend to increase in a long term. Moreover, interannual variation of meteorological condition is a huge influence on the variation of O_3 concentration. Therefore, it is difficult for observation to extract changes of O_3 concentration caused by reductions of NOx and VOC emissions. Therefore present study used numerical models to unify meteorological conditions.

The thesis comprises the following five Chapters.

In Chapter 1, the background, purpose, and structure of the thesis are described.

In Chapter 2, summaries of chemical reactions of O_3 and its precursors, as well as the models and emissions used in the present study, are described.

In Chapter 3, the results of evaluating the effect of emission controls on O_3 concentration in Kanto are described and discussed.

In Chapter 4, the results of the analysis of high concentrations of O_3 in the inland Kanto region are described and discussed.

In Chapter 5, the conclusions of the study are presented.

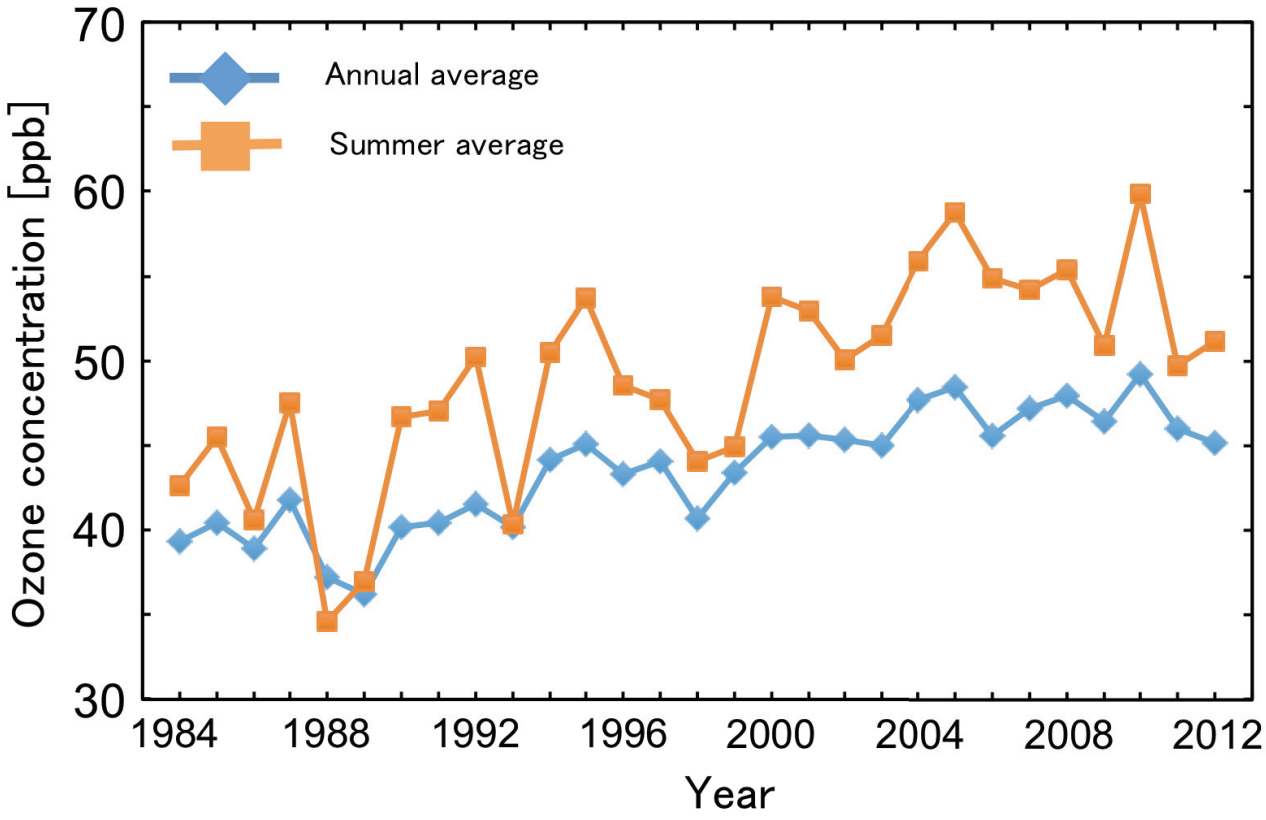

Fig. 1.3 Trends of annual and summer averages of daytime maximum O_3 concentration at general stations in Kanto region. Summer was defined as the period from June to September. Original data of these figures were obtained from the Atmospheric Environmental Regional Observation System.

2. Method

2.1 Model descriptions

2.1.1 Weather Research and Forecasting (WRF) model

In this study, Weather Research and Forecasting (WRF) model (WRF-ARW, Skamarock et al., 2008, Skamarock and Klemp, 2008) was used for meteorological simulations. WRF is a numerical model, which is supported by the Mesoscale and Microscale Meteorology Division in the National Center for Atmospheric Research. For the WRF simulations, meteorological and geometrical input data were preprocessed by the WRF Preprocessing System (the WPS). One of the subsystem of the WPS named geogrid defines horizontal resolutions of calculation domains and makes data including longitude and latitude, terrain height and land use of each grid. Terrain and land use data supplied by U.S. Geological Survey was used in this study. Another subsystem of the WPS named metgrid makes meteorological field data for input. This subsystem makes an input data on the horizontal calculation grids from reanalysis data (e.g. final analysis data provided by the National Center for Environmental Prediction; the NCEP or Mesoscale ANALysis (MANAL) data supplied by the Japan Meteorological Agency; the JMA) or data of sea surface temperature. Program real.exe makes data for initial and boundary condition and nudging based on the data made by the WPS. At last, program wrf.exe, the main program of WRF, calculates the process of meteorology based on the data made by real.exe program.

The physical process in the atmosphere was calculated by solving the compressible, nonhydrostatic flux form Eulerian equations on the vertical coordinate defined as

$$\eta = (P_h - P_{ht}) / (P_{hs} - P_{ht}) \qquad (2.2.1)$$

Here, P_h is the hydrostatic component of pressure and P_{hs} and P_{ht} (P_{ht} = constant) refer to values along the surface and top boundary. The definition (2.2.1) is proposed by Laprise (1992). η has a time dependency because P_h and P_{hs} are time dependent variable.

Eulerian equations can be expressed in the following equations (2.2.2) to (2.2.7) on the η vertical coordinate

$$\partial_t U + (\nabla \cdot Vu) - \partial_x(p\phi_\eta) + \partial_\eta(p\phi x) = F_U \qquad (2.2.2)$$

$$\partial_t V + (\nabla \cdot Vv) - \partial_y(p\phi_\eta) + \partial_\eta(p\phi y) = F_V \qquad (2.2.3)$$

$$\partial_t W + (\nabla \cdot Vw) - g(\partial_\eta p - \mu) = F_W \qquad (2.2.4)$$

$$\partial_t \Theta + (\nabla \cdot V\theta) = F_\Theta \qquad (2.2.5)$$

$$\partial_t \mu + (\nabla \cdot V) = 0 \quad (2.2.6)$$

$$\partial_t \phi + \mu^{-1}[(V \cdot \nabla \phi) - gW] = 0 \quad (2.2.7)$$

$$\partial_t Q_m + (\nabla \cdot VQ_m) = F_{Qm} \quad (2.2.8)$$

μ (x,y) represents the mass of dry air per unit area. V = μv = (U,V,W) and v = (u,v,w) are covariant velocities in the two horizontal and one vertical direction. Ω= μω, here ω represents the time derivative of η. Θ = μθ, here θ is defined as the potential temperature. p is the pressure, φ= gz is the geopotential, g is the gravity acceleration and Q_m = μq_m, here q_m is the mixing ratio of water vapor, rain, cloud etc…. Subscripts t, x, y and η in the equations (2.2.2) to (2.2.8) denote the differentiation. The third term on the left side of equations (2.2.2) to (2.2.4) means the pressure gradient. The right side of equations (2.2.2) to (2.2.5) and (2.2.8), F_U, F_V, F_W, F_Θ and F_{Qm} represent forcing terms arising from physical process, turbulent mixing, spherical projections and the earth's rotation. Equations (2.2.2) to (2.2.4) represent the equation of motion, equation (2.2.5) represents the conservation of potential temperature, equation (2.2.6) represents the mass conservation, equation (2.2.7) represents the variation of the geopotential and equation (2.2.8) represents the conservation of Q_m.

2.1.2 Community Multiscale Air Quality (CMAQ) model

In this study, the Community Multiscale Air Quality (CMAQ) model (Byun and Ching, 1999; Byun and Schere, 2006) was used for air quality simulations. Concentration of chemical matter (C) for each grid is expressed as follow

$$\partial_t C = R + E - L + \text{Advection} + \text{Diffusion}$$

Here, R represents the production and loss reaction, E represents the emissions, L represents the physically loss process (wet and dry deposition processes). These physical or chemical processes are calculated by using the data made by preprocessors shown in above sentence of this section.

In CMAQ, the Chemical Transport Model (the CTM) calculates behaviors of atmospheric materials such as chemical reaction, transportation deposition and etc… . The CTM calculations are based on meteorological data made by the Meteorology Chemistry Interface Processor (the MCIP), initial and boundary concentrations made by Initial and Boundary CONdition processors (ICON and BCON), clear sky photolysis rate calculator (JPROC) and emission data. MCIP extracts the meteorological data calculated by WRF. ICON and BCON may use a time-independent default data or calculated results of an outer domain. Results calculated by global chemical transport models (e.g. Model for OZone

And Related chemical Tracers; MOZART, Emmons et al., 2010) are also used. JPROC makes photodissociation reaction rate data for clear sky (i.e. no clouds) by latitude, altitude and hour angle. JPROC use the default data of vertical distribution of aerosol and O_3 concentration, temperature and pressure, absorption cross-section and quantum yield. CTM takes into account the effect of existence of clouds to the photodissociation reaction rate calculated by JPROC.

2.1.3 Emission data

For CTM calculation, emissions of NOx, VOCs, sulfer dioxide (SO_2), carbon monoxide (CO), PM_{10}, $PM_{2.5}$ were used. Domestic emission data for vehicles and the other sources were made on the basis of emission inventories prepared in the Japan AuTo-Oil Program (JATOP, Morikawa et al., 2012 for vehicle emissions and Nakatsuka et al., 2012 for the other sources). Ship emissions were derived from emission inventories developed by the National Maritime Research Institute (NMRI) and by the Ocean Policy Research Foundation (OPRF) (OPRF, 2012). Emissions in East Asia except Japan were produced from an emission inventory for Asia for year 2006 (the INtercontinental Chemical Transport Experiment phase B; INTEX-B, Zhang et al., 2009). The Regional Emission inventory in Asia (REAS, Ohara et al., 2007) were used for NH_3 emission. Biogenic VOCs (BVOC) emissions were estimated with the Model of Emissions of Gases and Aerosols from Nature (MEGAN, Guenther et al., 2006) version 2.04.

2.2 Model settings for the present studies

2.2.1 The evaluation of effect of emission control for O_3 concentration in Kanto

Model settings are described in this sub-section for the evaluation of effect of emissions reductions on the O_3 concentration. The calculation period was set from 25 December, 2004 to December, 2005. The first seven days were used for spin up. Spin up period is a calculation period required for the disappearance of effects of the initial condition. Four months from June to September, 2005, were analyzed to evaluate the effect of emission controls on high concentration O_3 in daytime. As shown in Figure 2.1, the model was set for three domains of D1, which covers a wide area of East Asia, D2, which mostly covers the four majour islands of Japan, and D3, which focuses on the Kanto region.

Four diagnostic points, Isesaki in Gunma Prefecture, Kumagaya and Oomiya in Saitama Prefecture, and Shinjuku in

Tokyo metropolis, were chosen in order to evaluate whether calculated concentrations reproduce observed concentrations and to analyze effects of emissions reductions on O_3 concentration. Confirmation of the reproducibility is required to ensure the validity of the analysis with outputs of emission-changed simulations. These four points were located along the main path of sea breezes.

In the WRF simulation, the horizontal resolutions were 64 km, 16 km and 4 km. The numbers of grids were 108×92, 116×124, and 72×72 for D1, D2, and D3, respectively. The number of vertical layers was 30. As input data to WRF final analysis data provided by NCEP for meteorology and Optimum Interpolation Sea Surface Temperature (OISSTHR; Reynolds et. al, 2007) provided by the National Oceanic and Atmospheric Administration (NOAA) for sea surface temperature were used. The WRF model was configured with Janjic (2002)'s planetary boundary layer model, the WRF single-moment 6-class microphysics scheme (Hong and Lim, 2006), the Kain-Fritsch cumulus parameterization scheme (Kain, 2004) for D1 and D2, the Noah land surface model (Chen and Dudhia, 2001), the Rapid Radiative Transfer Model for GCMs (RRTMG) long and short wave radiation scheme (Iacono et al., 2008). In the CMAQ simulation, horizontal resolutions of D1 to D3 are same as WRF simulation. To exclude meteorological results influenced by lateral boundaries, CMAQ domains were set by a few grids inside the WRF domains. The number of grids are 80×96, 108×100, and 56×56 for D1, D2 and D3, respectively. Hourly WRF outputs were processed by MCIP. The model of gas phase chemistry used in CMAQ simulations was SAPRC-99 (Carter, 2000). For initial and boundary conditions of the base case CMAQ calculation, the default value of CMAQ was used for D1, and simulated results for the outer domains D2 and D3. Emission data described in section 2.2.3 was used. In this evaluation, 2000 and 2005 were selected as target years. Table 2.1 shows total amounts of the anthropogenic O_3 precursors (NOx and VOC) emitted in D3 in 2000 and 2005. The NOx emission was reduced by about 5.3% and the VOC emission was reduced by about 16.3% in 2005 compared to 2000. Figure 2.2 shows distributions of the anthropogenic NOx and VOC emissions and changes in those emissions from 2000 to 2005. High emissions of NOx are distributed in and around central Tokyo. VOC emissions are distributed similarly with the NOx emissions, but there are also high emissions in inland Kanto, around Kumagaya and Isesaki (points of these two locations are shown in Fig. 2.1). As shown in Fig. 2.2, reductions of emissions in the metropolitan area are particularly significant for both VOC and NOx. In addition, there are areas where the VOC emission has been reduced greatly in inland. In this study, three cases of simulations were conducted by changing the anthropogenic emissions in Japan (Table 2.2).The base case has less NOx and VOC emissions compared

to the NOx2000_VOC2005 and NOx2005_VOC2000 cases, respectively. Therefore, [Base case O_3 Conc.] – [NOx2000_VOC2005 O_3 Conc.] is defined as “NOx reduction case” and [Base case O_3 Conc.] – [NOx2005_VOC2000 O_3 Conc.] is defined as “VOC reduction case”. Moreover, in comparison with the NOx2000_VOC2000 case, the base case has less emissions of both NOx and VOC. For this reason, [Base case O_3 Conc.] – [NOx2000_VOC2000 O_3 Conc.] is regarded as simultaneous reductions of the NOx and VOC emissions. For all the emission reduction cases, calculation conditions like meteorological fields, initial and boundary conditions for D_3, BVOC, and anthropogenic emissions out of Japan were common to the base case. In this study, high O_3 criterion was defined as 120ppb, in accordance with the standard criterion for photochemical oxidant advisories in Japan.

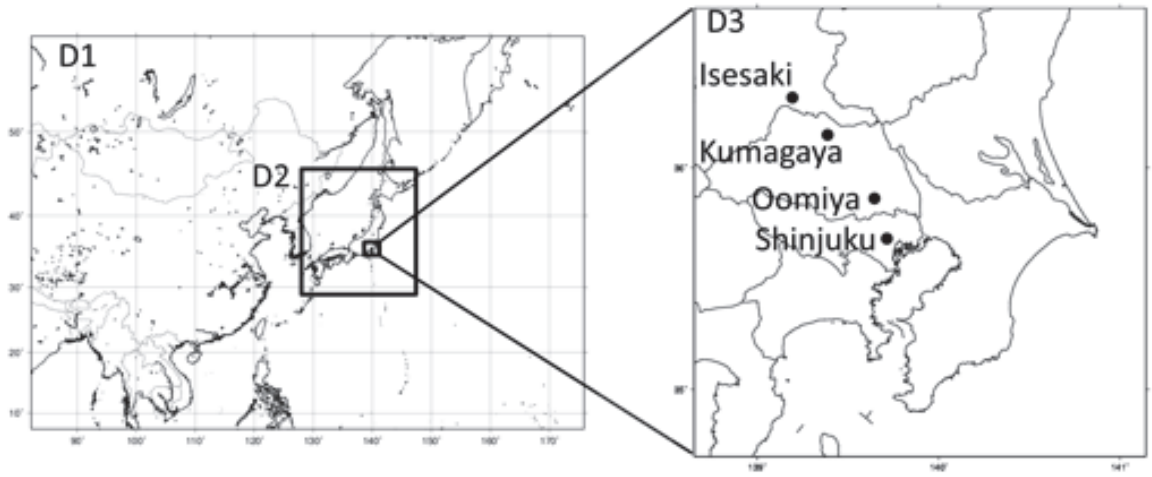

Fig. 2.1 Horizontal model domains for CMAQ. Black points in D3 indicate locations of diagnostic points in Kanto; Isesaki, Kumagaya, Oomiya and Shinjuku. (This figure was derived from Kiriyama et al. accepted byJournal of Japan Society for Atmospheric Environment.)

Table 2.1. Emission of anthropogenic NOx and VOC in 2000 and 2005 in D3.

Precursor	Emission in ‘00	Emission in ‘05	Variation from ’00 to ‘05
NOx [10^{10}g]	15.1	14.3	-0.8
VOC [10^{10}g]	19.6	16.4	-3.2

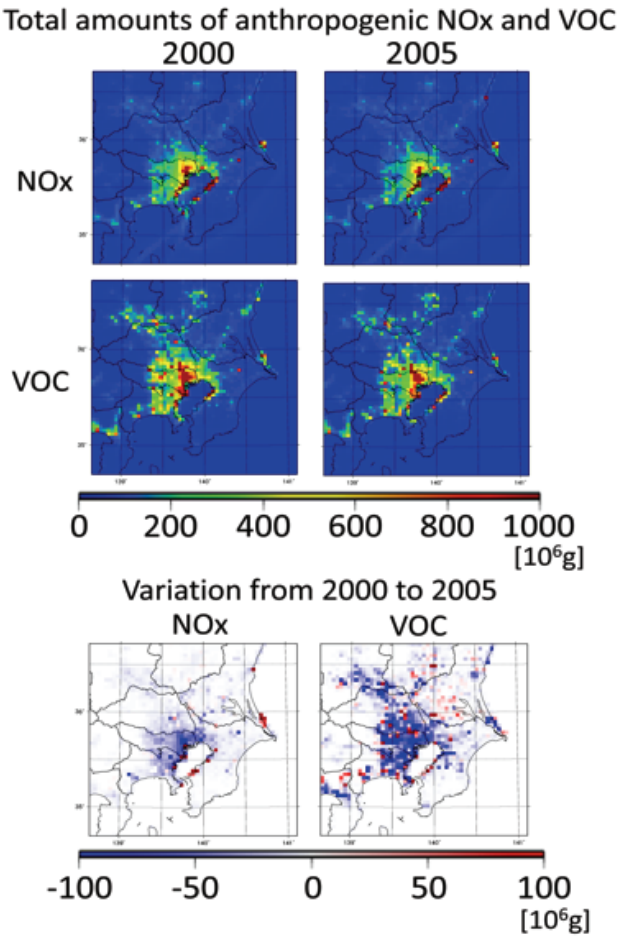

Fig. 2.2 Distributions of total amounts and variation of anthropogenic NOx and VOC in analysis period in Kanto of Japan. (This figure was derived from Kiriyama et al. accepted byJournal of Japan Society for Atmospheric Environment.)

Table 2.2 Combination of anthropogenic emission data year and calculation cases.

Calculation case	Combination of Emission data year
Base case	NOx:2005 VOC:2005
NOx2000_VOC2005	NOx:2000 VOC:2005
NOx2005_VOC2000	NOx:2005 VOC:2000
NOx2000_VOC2000	NOx:2000 VOC:2000

2.2.2 The clarification of causes for high concentration ozone in inland Kanto

In this sub-seciton, model settings are described for simulations to find out causes for high concentration O_3 in inland Kanto. The calculation period was from 16 July to 8 August, 2010. The first four days were used for spin up. The model was set for three domains same as shown in section 2.2.1 (Figure. 2.3). In the WRF simulation, the horizontal resolutions were same as those shown in section 2.2.1, but the number of grids were 109×93, 73×73, and 97×97 for D1, D2, and D3, respectively. The number of vertical layers was 30. As input data to the WRF model, final analysis data provided by NCEP, and MANAL data provided by JMA (used for D2 and D3) for meteorology, and real-time global sea surface temperature analysis data provided by NOAA/NCEP for sea surface temperature were used.

In the CMAQ simulation, horizontal resolutions of D1 to D3 were same as WRF simulation and the number of grids were 80×96, 56×56, and 72×72 for D1, D2 and D3, respectively. For initial and boundary conditions of the CMAQ calculation, the results calculated by MOZART4/The Goddard Earth Observing System model, version 5 (GEOS-5) (Emmons et al., 2010) were used for D1, and simulated results were used for the outer domains D2 and D3. In this calculation, the gas phase chemistry model and meteorological preprocessor were used SAPRC-99 and MCIP.

To conduct two other simulations than the base case, the Kanto region was divided into two areas. (Fig. 2.3). One is the interior of a circle, wihich is mostly corresponding to Route 16 with radius about 40 km and centered at central Tokyo (labeled “metropolitan” in Fig. 2.3). The other area is the exterior of this circle (named “non-metropolitan”). In the simulations, “metropolitan case” means a simulated case with no emissions in the metropolitan area, and “non-metropolitan case” means another simulated case with no emissions in the non-metropolitan area. Table 2.3 summarizes the amounts of emissions in the metropolitan and non-metropolitan area, and the total amount of emissions in D3. Table 2.3 shows that precursors emitted in the metropolitan area include 6.90×10^{9} g of NOx, and 1.61×10^{10} g of VOCs over the calculation period, accounting for approximately 40% of the total NOx and VOC emissions. The non-metropolitan area emits more precursors than the metropolitan area. However, when compared emissions per unit area, the metropolitan area emits much more precursors than the non-metroplian area. Contributions of emissions in the metropolitan are/the non-metropolitan area were calculated as difference in the O_3 concentrrations between the base case and the metropolitan case/the non-metropolitan case. If the O_3 concentration increases under no chemical reactions, the increase is thought to be influenced by horizontally or vertically transported O_3. Moreover, the increase of O_3 is largely influenced by vertically transported O_3 if horizontal distributions of O_3 are almost uniform, and wind speeds are

slow. Therefore, to evaluate the effect of downward transport of residual O_3 in the upper atmosphere on ground-level O_3 concentrations, we also conducted another simulation with no chemical reactions (No_chem). In the No_chem case, the simulation starts at 05:00 Japan Standard Time (JST, UTC + 9 hours; hereinafter time is given as JST) with the base case results of D3 as initial conditions. This simulation stops at 05:00 on the next day. For all calculations, the boundary conditions were common to the base case. Initial condition of the base case was applied to the metropolitan and non-metropolitan cases. Term “Inland areas” were used in the sense of areas in and around Kumagaya and the north. A criterion for high concentration O_3 is also defined as 120ppb for the same reason as described in section 2.2.1.

2.3 Observational data

Observed O_3 concentration data used in this study were obtained from the Atmospheric Environmental Regional Observation System (AEROS, http://www.nies.go.jp/igreen/). This data set is same as Ministry of Environment (2014), which was used for the analysis of trends of O_3 and its precursors.

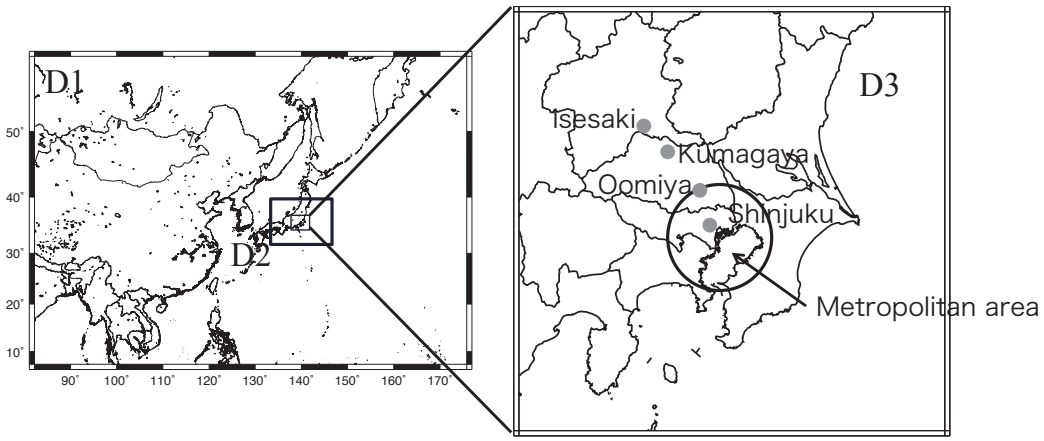

Fig. 2.3 Horizontal model domains used for CMAQ. The black circle divides the Kanto region into two areas, a metropolitan area (inside area of the circle) and a non-metropolitan area (outside area of the circle). Black circle was defined by reference to Route16. Gray points indicate locations of diagnostic points in Kanto: Isesaki, Kumagaya, Oomiya, and Shinjuku. (This figure was derived from Kiriyama et al. accepted by Asian Journal of Atmospheric Environment.)

Table 2.3 Total amounts of precursors emitted from D3, and amounts of precursors emitted from metropolitan area and non-metropolitan area over the calculation period.

Emission area	NOx Amounts (g/25 days)	VOCs Amounts (g/25 days)
D3-wide	1.83×10^{10}	8.27×10^{10}
Metropolitan area	6.90×10^{9} (about 38% of D3-wide)	1.61×10^{10} (about 37% of D3-wide)
Non-Metropolitan area	1.14×10^{10} (about 62% of D3-wide)	6.66×10^{10} (about 63% of D3-wide)

3 Evaluation of effects of emission reductions on concentration of O_3 in Kanto

3.1 Reproducibility of the calculation and diurnal variation of O_3 concentration in the high concentration day

Figure 3.1 shows the comparison of observed and simulated daytime maximum concentration of O_3 in high concentration days at four points shown in Fig. 2.1. From Fig. 3.1, there is a tendency of overestimation regarding the average of the daily maximum value. On high concentration days, seven data exceeded the factor 2, but most data were within the factor 2. Therefore, the base case has good reproducibility of observed O_3 concentration in high concentration days and can be used for evaluations of emissions reductions.

Figure 3.2 shows the distributions of O_3 concentrations in D3 on 28 July 2005, one of high concentration days. Transport from the coastal area to the inland area driven by sea breeze was shown on this day. It is well known that the transportation of pollutants by sea breeze strongly influences O_3 concentrations in Kanto (e.g. Yoshikado, 2007). In the early morning, O_3 concentrations were low over the whole region, especially around the coast of Tokyo Bay. At noon, O_3 concentration was increased mainly by photochemical production. At this time, pollutants from the coastal area have not reached inland Kanto. One of the reasons for this phenomenon will be shown in chapter 4. In the afternoon, winds from the sea flow in the coastal area of southwest Kanto. Also over the Tokyo Bay, the sea breeze has begun to approach towards the land. Pollutants emitted from sources along the coast caused high-concentration O_3 in the inland area.

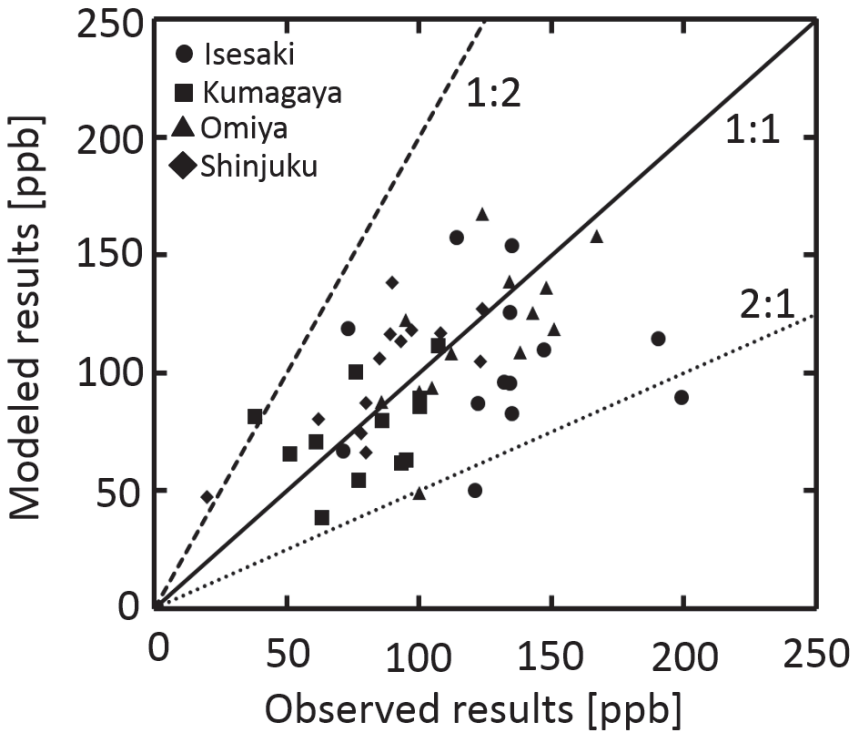

Fig. 3.1 The Scatter plot of observed versus simulated daytime maximum O_3 concentration in the high concentration days. (This figure was derived from Kiriyama et al. accepted byJournal of Japan Society for Atmospheric Environment.)

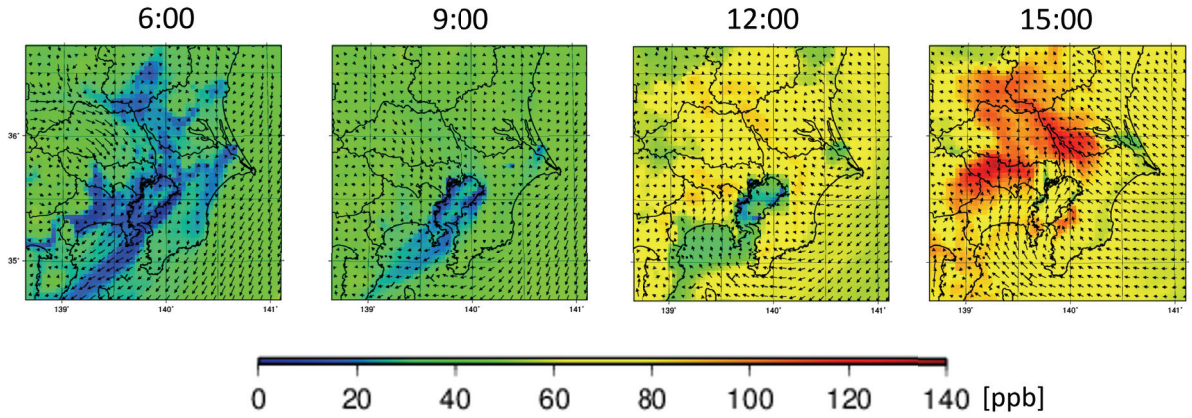

Fig. 3.2 Distributions of O_3 concentration and wind simulated by Base case in 28 July 2005.

(This figure was derived from Kiriyama et al. accepted byJournal of Japan Society for Atmospheric Environment)

3.2 Changes of O_3 daytime maximum from 2000 to 2005

Figure 3.3 shows the variation of monthly averaged daytime maximum concentration of O_3 in each emission reduction case (NOx reduction case, VOC reduction case and NOx and VOC emisson reduction case; these were described in the section 2.2.1) at Isesaki, Kumagaya, Oomiya and Shinjuku. As shown in Fig. 3.3, in NOx and VOC emissons reduction case, O_3 concentration always showed a decrease at Isesaki and Kumagaya. At Oomiya, O_3 concentration increased slightly in June but decreased in subsequent three months. On the other hand, O_3 concentration had increased during the analysis period at Shinjuku. Therefore, it is suggested that the daytime maximum concentration of O_3 will be decreased in a wide area of Kanto by only the effect of reduction of NOx and VOC emissions. At Isesaki in the NOx reduction case, it is shown that O_3 concentration tends to decrease in July and August, and tends to increase in June and September. O_3 concentrations in other three points increased in the NOx reduction case. There was a difference in increment between Kumagaya and Shinjuku up to about 3ppb. On the other hand, daytime maximum concentration of O_3 decreased in the VOC reduction case in these four points.

Figure 3.4 shows the distribution of changes in the O_3 concentration from the base case for the variation averaged (a) in the overall analysis period, (b) in July and (c) in the high concentration days in July. In the NOx and VOC emission reduction case, O_3 concentrations decreased in Kanto except for central Tokyo (around Shinjuku). The area where O_3 concentrations increased corresponds well to the area with very high NOx emissions along the coastal area of Tokyo Bay. Therefore, the area where O_3 concentrations increased was strongly affected by NOx emissions reduction. From the distributions of the NOx reduction case, increases in O_3 concentrations can be seen in a wide range of the Kanto region. In particular, the tendency of the increase is greater in the coastal area of the Tokyo Bay than the central part of Kanto. On the other hand, O_3 concentrations tend to decrease over most of Kanto in VOC reduction case. Moreover, O_3 concentrations decreased significantly around Oomiya on the high concentration days. Figure 3.5 shows the changes of O_3 concentration between base case and NOx and VOC emission reduction case averaged all over the ground level layer and from the ground level to the 10^{th} layer in D3. The 10^{th} layer is at the altitude of about 2000 m, the top of PBL in summertime. From Fig. 3.5, O_3 concentrations in bottom layer decreased in summertime as Fig. 3.4 shows. O_3 concentrations from the ground level to the top of PBL also decreased in summertime between 2000 and 2005. Therefore, not only on the ground level but also the upper air, O_3 concentration was decreased by the reduction of NOx and VOC emissions.

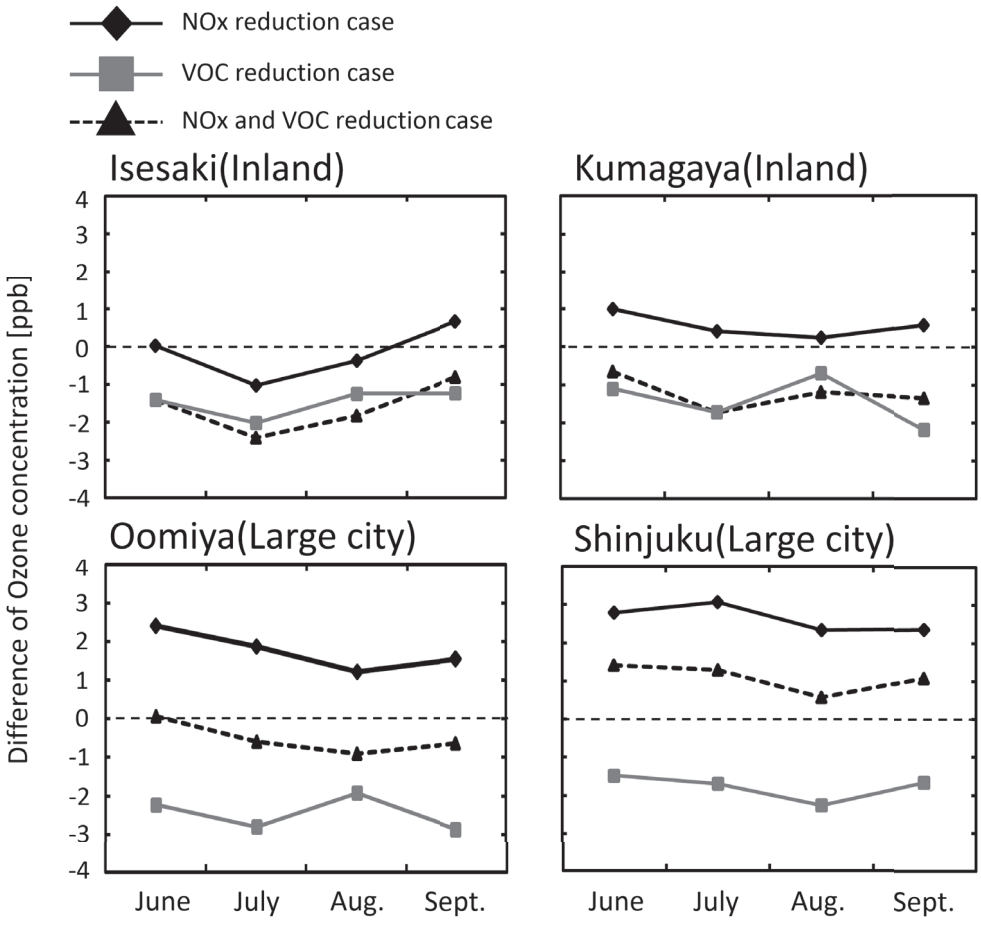

Fig. 3.3 Monthly variations of O_3 concentration between each emission reduction case and base case

Position of these four points was shown in Fig. 2.1

(This figure was derived from Kiriyama et al. accepted byJournal of Japan Society for Atmospheric Environment)

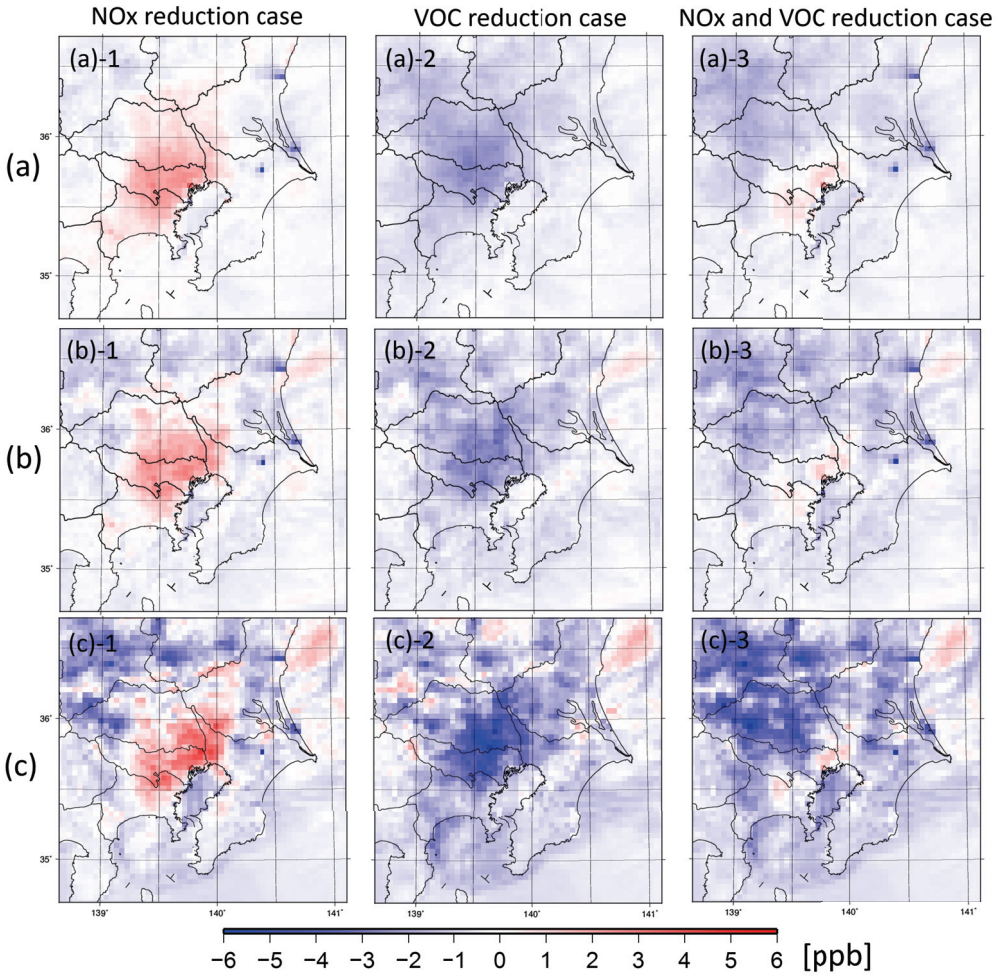

Fig.3.4 The distributions of anomalies of averaged daytime maximum O_3 concentration between Base case and each emission case

(a) : Averaged in entire analysis period, (b) : Averaged in July and (c) : Averaged in high concentration days in July.

(This figure was derived from Kiriyama et al. accepted byJournal of Japan Society for Atmospheric Environment)

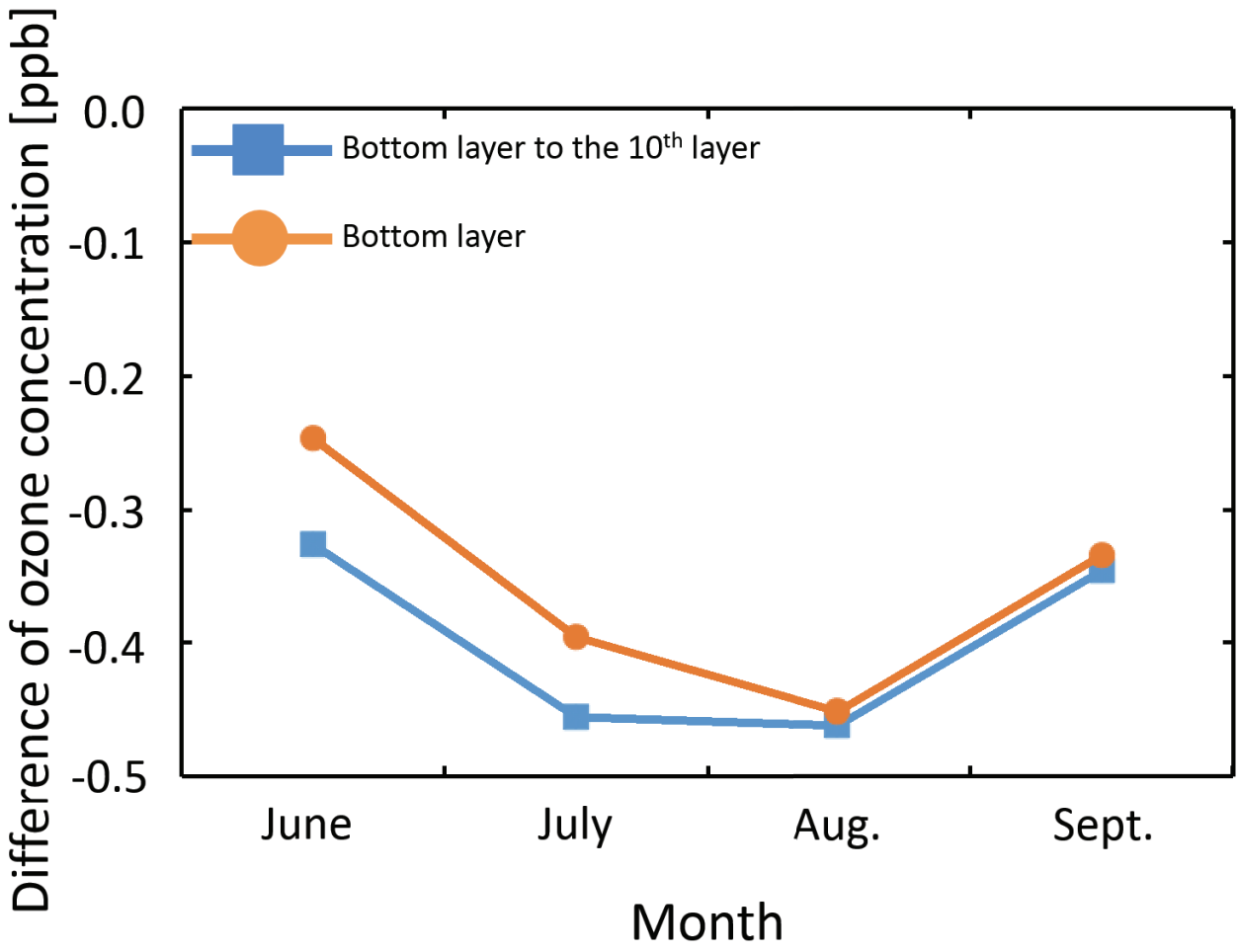

Fig. 3.5 Monthly variations of O_3 concentration between NOx and VOC emission reduction case and base case. Bottom layer indicates that O_3 concentration averaged all over the bottom layer (the ground level) of D3 in each month. Bottom to the 10^{th} layer indicates that O_3 concentration averaged all data from the ground level to 10^{th} layer of D3.

3.3 Changes in particular points of each month

There was a large difference in the north-south concentration variation in the NOx reduction case between Isesaki, Kumagaya and Oomiya where O_3 concentrations were decreased in the NOx and VOC simultaneously reduced case. But there was no significant difference on variation of O_3 concentration between the points in the VOC reduction case as shown in the NOx reduction case. Therefore, it is considered that the VOC emissions reduction have the effect of decreasing O_3 concentration uniformly in month average. Large difference occurs in the amount of decrease of NOx emissions when compared to inland area, Kumagaya and Isesaki and central Tokyo, around Shinjuku. But there is no great difference in VOC emissions as NOx emission indicated when compared with the surrounding central Tokyo and inland, around Isesaki and Kumagaya as shown in Fig. 2.2. Therefore, it is considered that reductions in the O_3 concentrations found in the NOx and VOC emission reduction case were influenced by reducing emissions of VOC. Moreover, differences in amounts of decrease of O_3 concentration for each point was caused by reduction of NOx emissions.

As shown in section 1.2, O_3 production can take two states, the NOx sensitive and VOC sensitive regime depending on the combination of NOx emissions and VOC emissions. Moreover, Sillman et al. (1998) shows that there is a state in which the O_3 concentration decreases by reducing both the NOx and VOC emission (Mixed sensitive regime). From Fig.3.3, Isesaki is in the mixed sensitive regime because the O_3 concentrations were decreasing in both the NOx reduction case and VOC reduction case in July and August. The VOC sensitive regime predominated at Isesaki in June and September because O_3 concentrations increased by 0.2 ppb and 0.02 ppb in the NOx reduction case but decreased in these two months in the VOC reduction case. It is presumed for three points other than Isesaki that these points are often in the VOC sensitive regime when O_3 concentrations increased in the NOx reduction case and decreased in VOC reduction case.

3.4 Changes over the Kanto region of Japan

In the coastal area with high emissions, it is expected to be in the state of VOC sensitive regime for the daytime maximum O_3 concentration, because O_3 concentrations decreased in the VOC reduction case and increased in the NOx reduction case, as shown in section 3.3. Meanwhile, when an attention is paid to Kumagaya and northward, O_3 concentrations increased over the area up to approximate latitude of Isesaki in an average of the entire analysis period

and one month in July in the NOx reduction case. In addition, O_3 concentrations decreased in the north of Isesaki. On the other hand, in the VOC reduction case, the area where O_3 concentrations decreased spreaded over inland Kanto. In inland Kanto, one of factors for decrease of O_3 concentrations is reduction in the amount of NOx transported from coastal area with high NOx emissions to inland. Daytime maximum concentration of O_3 increased over a large area in the NOx reduction case, but the increase was limited in a portion of central Tokyo in the NOx and VOC emisson reduction case. Therefore, it can be considered in the comparison between 2000 and 2005 that the NOx reduction affects for the increament of daytime maximum concentration of O_3 in central Tokyo. In consideration of the O_3 sensitivity regime, it is expected that the coastal area was in the state of VOC sensitive regime, and the reduction of VOC emissions were effective for the decrease in O_3 concentrations. Reduction of the NOx and VOC emissions affects decreases in the daytime maximum concentrations of O_3 in inland Kanto. It is considered that inland Kanto was in the state of mixed sensitive or VOC sensitive regime.

3.5 Ozone sensitivity to NOx and VOC emissions in high concentration days

The relationship between the variation of O_3 concentration and each emission reduction cases were mentioned. There were noted features and effects of each emission reduction case for the differences of daytime maximum concentration of O_3. In this section, we try to grasp the feature of effects of reductions of NOx and VOC emissions on O_3 concentration by using the O_3 sensitivity regime, which is used by Sillman and He (2002). Locations have been classified according to the following definitions which were derived from Sillman and He (2002),

(1) VOC sensitive regime: O_3 concentrations in the NOx2005_VOC2000 case are higher than those in both the base case and the NOx2000_VOC2005 cases at a specific hour by at least 3 ppb.

(2) NOx sensitive regime: O_3 concentrations in the NOx2000_VOC2005 case are higher than those in both the base case and the NOx2005_VOC2000 cases at a specific hour by at least 3 ppb.

(3) Mixed sensitive regime: The NOx2000_VOC2005 and NOx2005_VOC2000 cases have O_3 concentrations within 3 ppb differences from each other, and both have O_3 concentrations higher than those in the base case by at least 3 ppb.

(4) Titration: O_3 concentrations in the base case is higher than those in the NOx2000_VOC2005 case by at least 3ppb, and O_3 concentrations in the NOx2005_VOC2000 case are less than by 3ppb compared to the base case.

(5) Insensitive: Other cases.

Sillman and He (2002) set NOx and VOC reduction rates as 35% and 25%, respectively. However, in this study, NOx reduction rate is about 6% and VOC reduction rate is about 20% as shown in Table 2.1. Therefore, differences in O_3 concentrations between each case are expected to be small. So, the threshold value was defined as 3 ppb. Analyses of the regimes were conducted by focusing on high concentration days. Figure 3.6 shows an example of the distribution of regimes on 28 July, one of the high concentration O_3 days. The titration regime appears in coastal area of Tokyo Bay at 7:00. This area corresponds to an increasing area of O_3 concentrations, and weakening of the titration effect by NOx seems to affect the increase in O_3 concentrations at this time. The titration regime partially exists in the area surrounding central Tokyo at 12:00, but VOC sensitive regime distributed mainly in the area. Therefore, it is likely that decrease of the O_3 concentration is due to the reduction of the VOC emissions. In addition, the mixed sensitive or NOx sensitive regimes appeared in inland Kanto at 17:00, when sea breeze has reached to inland Kanto. Figure 3.6 also shows the distribution of the regime for daytime maximum concentration of O_3. From the map for daytime maximum concentratioin of O_3 in Fig. 3.6, the VOC sensitive regime distributed surrounding of central Tokyo. At the same time, the mixed sensitive or NOx sensitive regime sparsely exists in inland. Inoue et al. (2010) showed that the VOC sensitive regime distributed only in a part of central Tokyo, and the regime changes from mixed sensitive to NOx sensitive regime toward inland. In addition, the NOx sensitive regime is distributed in most of the Kanto area, as described by Inoue et al. (2010). Also in the present study, the VOC sensitive regime distributed in the surrounding central Tokyo and the NOx sensitive regime distributed in inland Kanto. However, changes in the regime in relatively short ranges, which was highlighted by Inoue et al. (2010), have not been seen in this study. Also, the NOx sensitive regime distributed spindliler compared to Inoue et al. (2010).

Figure 3.7 shows the numbers of occurrences of each regime for the daily maximum concentration of O_3 in the four sites shown in Fig. 2.1. Fig. 3.7 indicates data in the top ten days when O_3 over 120 ppb widely distributed over Kanto region in the base case. These ten days are 21, 25, 26 June, 18, 21, 29, 31 July, 3 August, 2 and 3 September. According to Fig. 3.6, Shinjuku and Oomiya often located in the VOC sensitive regime, while Isesaki and Kumagaya mainly located in the mixed sensitive or NOx sensitive regime rather than the other regimes.

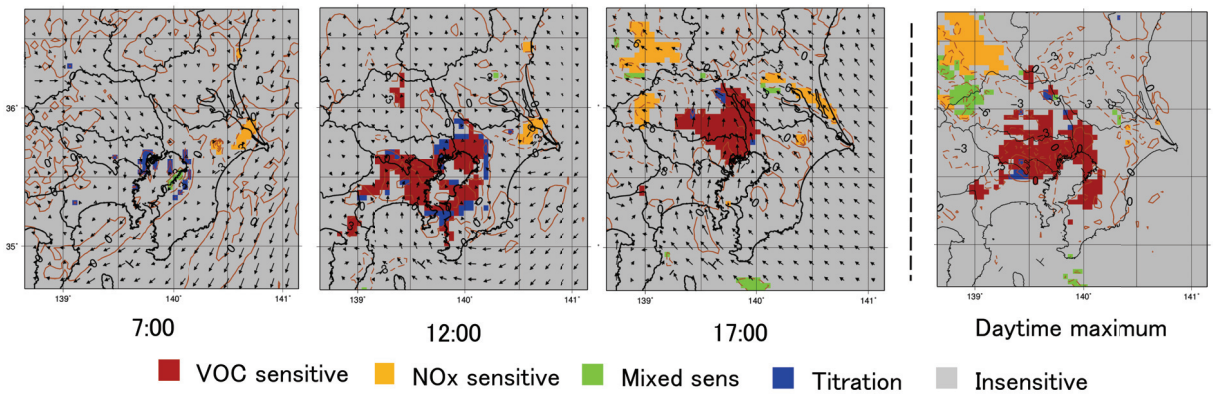

Fig. 3.6 The distributions of O_3 sensitivity regime and anomalies of O_3 concentration between the base case and the NOx2000_VOC2000 case in 28 June. Orange solid lines in the Figure indicate the positive anomaly and dashed line indicate negative anomaly. Numbers shown in the Figure indicate the value of variation of O_3 concentration.

(This figure was derived from Kiriyama et al. accepted byJournal of Japan Society for Atmospheric Environment)

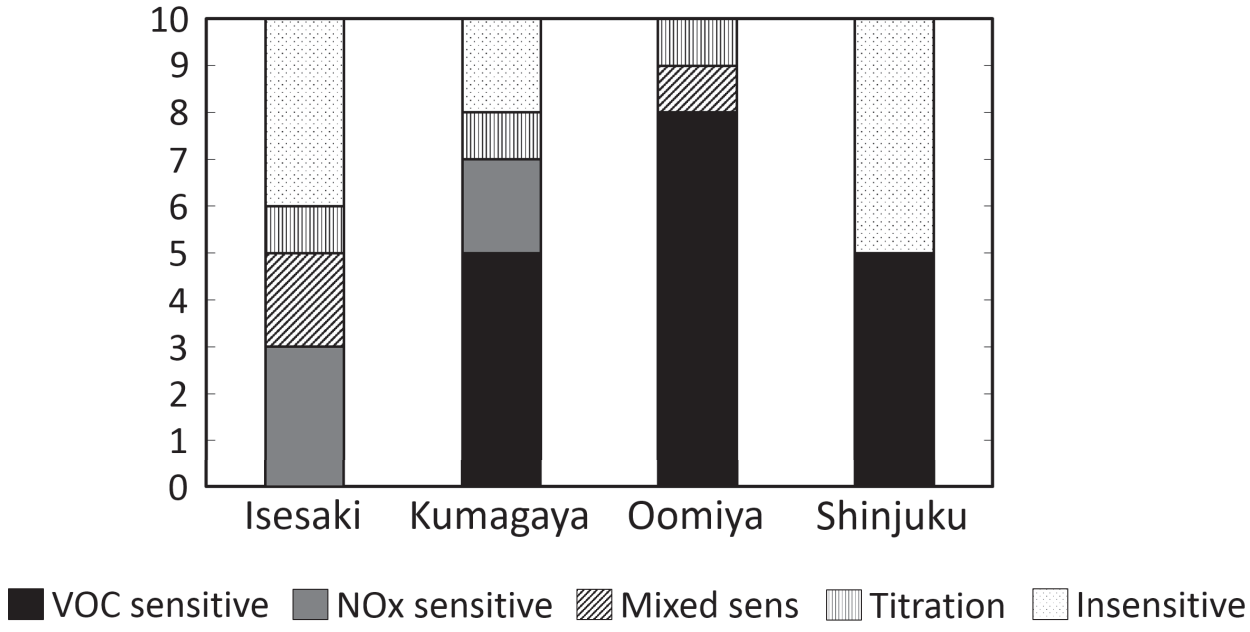

Fig. 3.7 Numbers of incidence of each O_3 sensitive regime in the top 10 days exceeding the 120ppb had appeared.

(This figure was derived from Kiriyama et al. accepted byJournal of Japan Society for Atmospheric Environment)

3.6 Conclusion of Chapter 3

Effects of the anthropogenic NOx and VOC emission reductions on daytime maximum of O_3 concentrations were examined by use of the WRF and the CMAQ models. The NOx and VOC emissions reductions between 2000 and 2005 resulted in increase in O_3 daytime maximum in and surrounding area of central Tokyo. But in other areas, emission reductions works effectively to decrease daytime maximum concentration of O_3. Daytime maximum of O_3 concentration increased in a wide area of the plains in the NOx reduction case. On the other hand, O_3 concentration decreased in the entire Kanto region due to reduction in VOC emissions. Therefore, reductions of VOC emissions effectively work for decreases in O_3 concentrations. In addition, O_3 concentrations were lowered by either reduction of VOC or NOx emissions in inland Kanto. It is considered that O_3 productions decreased with decline in amounts of O_3 precursors transported from central Tokyo by sea breezes and emissions from inland sources. According to the distribution of O_3 sensitivity regimes on high concentration days, O_3 concentration was increased by weakening of titration effect by NOx in the surroundings of central Tokyo in the early morning. But in the afternoon, VOC sensitive regime covered surrounding area of central Tokyo and NOx sensitive or mixed sensitive regime has appeared in inland. Occurrences of each regime on the highest ten days of the high concentration days shows that mixed sensitive and NOx sensitive regimes accounted for half of the number of occurrences in Isesaki, and VOC sensitive and NOx sensitive regimes predominated in Kumagaya. Therefore, emission reductions of VOC and NOx are effective for decrease in O_3 concentration in inland Kanto. On the other hand, VOC sensitive regime is the majority in large cities such as Shinjuku and Oomiya, and therefore VOC emissions reductions are effective on decrease in O_3 concentration in coastal, large city area. The results of present study show the effectiveness of the reduction of precursors to the decrease of O_3 concentration in each area of Kanto.

4. Increase in O_3 concentration in the morning in inland of the Kanto region

4.1 Temporal change in O_3 concentration and reproducibility of base simulation results

Figure 2.3 shows the locations of Shinjuku in metropolitan Tokyo, Oomiya and Kumagaya in Saitama Prefecture, and Isesaki in Gunma Prefecture. These four points are located on the main approach path of sea breezes and are used as representative locations for observing O_3 concentrations. Isesaki and Kumagaya are representatives of inland area and Shinjuku and Oomiya are representatives of coastal and large city area. Figure 4.1 shows a time series of observed and base simulation results at Shinjuku, Oomiya, Kumagaya, and Isesaki. As shown in Fig. 4.1, two south points and inland points have different diurnal pattern. Observed O_3 at two south points have one daily peak, and two inland points have two daily peaks, especially in the early days of the study period. Figure 4.2 shows the hourly averaged O_3 concentration at two inland points. The averaging period is from 20 to 24 July. In the period, high concentration O_3 has continuously occurred. As shown in Fig. 4.2, variation in simulated concentration at Kumagaya shows two daily peaks. The first peak appeared at 13:00 and the second peak appeared at 18:00. At Isesaki, daytime maximum concentration occurred at 15:00 and the second peak appeared at 20:00. In inland area in the high concentration days, O_3 concentration can take two daily peaks. Comparing the observed and base simulation results, the base simulation at Kumagaya and Oomiya overestimated observed O_3 concentrations, especially in the latter half of this period. For nighttime data, results of the base simulation at all four points overestimated the observed results, but simulations and observations are in good agreement for daytime temporal variation. At Isesaki, peaks of O_3 concentrations are also well estimated by the base simulation. The scatter plots in Figure 4.3 show that the base simulation correlates well with observations. The base simulation overestimated more than twofold at the low concentration field, which corresponds to nighttime data. At these four points, O_3 concentrations were above 120 ppb for several days of observation and base simulation data. In particular, from 20 to 24 July high O_3 concentrations continuously occurred in the inland Kanto region. O_3 concentrations were low at Shinjuku and Oomiya from 5 to 8 August, but O_3 concentration increased up to about 80 ppb at Kumagaya and Isesaki during this period. This study focuses on high O_3 concentration in the inland Kanto region, so we analyzed contributions for high concentration O_3 in these two periods.

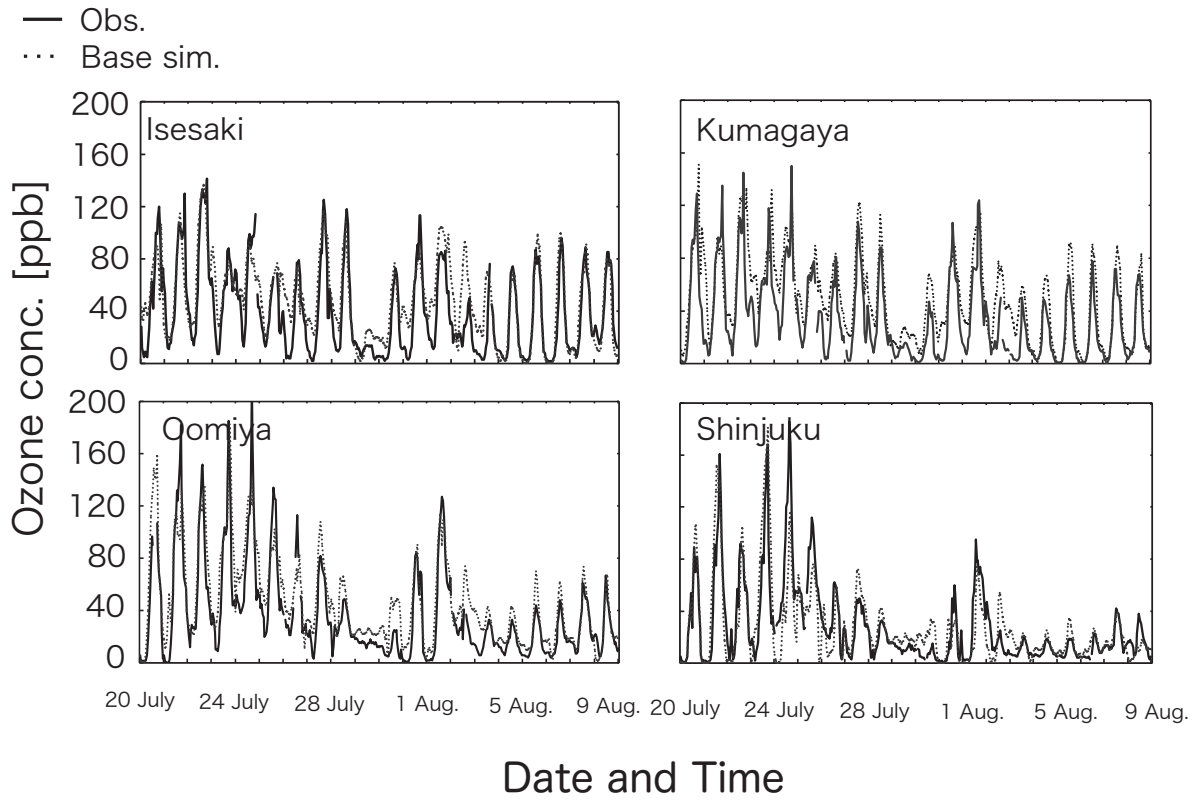

Fig. 4.1 Time series of O_3 concentration of observed and base case simulation results at points shown in Fig. 1. Solid lines indicate observed O_3 concentrations and dotted lines indicate base case simulation results. (This figure was derived from Kiriyama et al. accepted by Asian Journal of Atmospheric Environment)

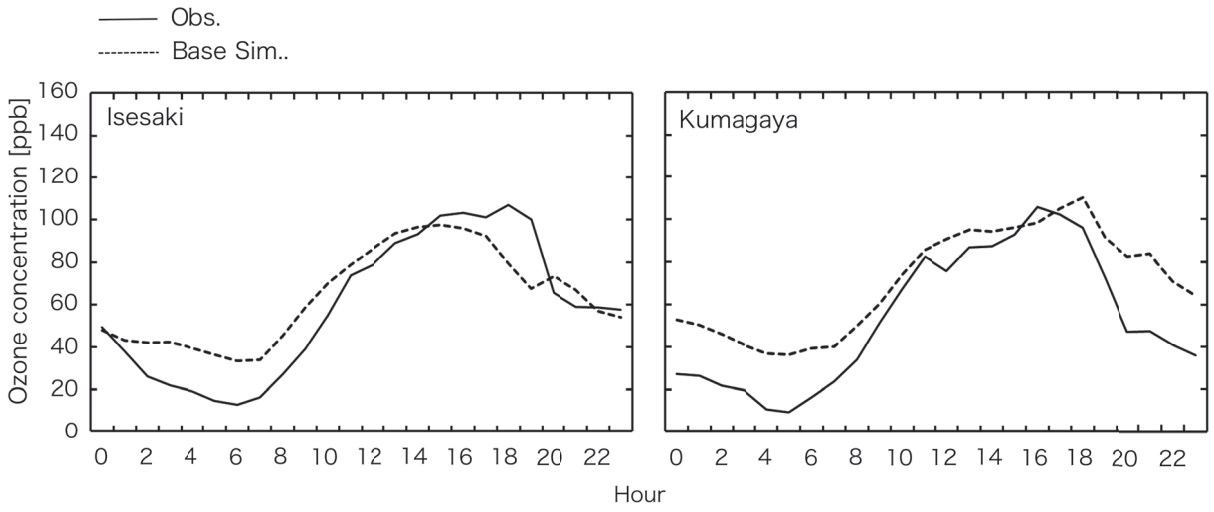

Fig. 4.2 Hourly averaged O_3 concentrations at Isesaki and Kumagaya. Averaged period is from 20 to 24 July. (This figure was derived from Kiriyama et al. accepted by Asian Journal of Atmospheric Environment)

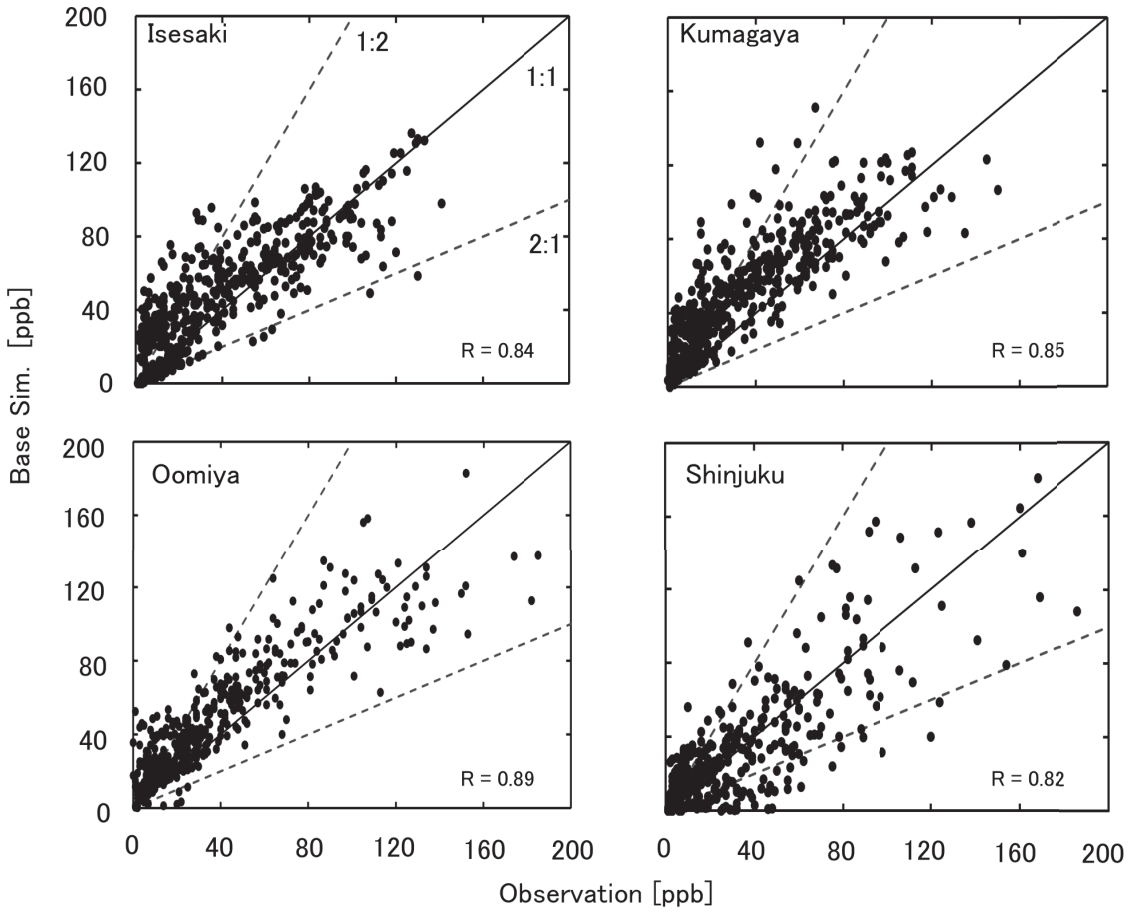

Fig. 4.3 Scatter plots of observed versus simulated O_3 concentration for the period from 20 July to 8 August at the points shown in Fig. 1. R shown in each plot is correlation coefficient. (This figure was derived from Kiriyama et al. accepted by Asian Journal of Atmospheric Environment)

4.2 Contribution of emission areas for the inland Kanto region

4.2.1 Period from 20 to 24 July

Figure 4.4 shows a time series of the base simulation and the contribution of the metropolitan and non-metropolitan areas for O_3 concentrations at Isesaki and Kumagaya from 20 to 24 July. In this and the following corresponding figure, there are differences between the base simulation results and the sum of contributions. The differences are caused by transport of O_3 and its precursors from the outer domain. Also, the nonlinear relationship between O_3 concentrations and amounts of emitted precursors is another cause of the differences. The additional sensitivity simulations that set the emission reduction rates to 50% and 20% in metropolitan and non-metropolitan area were also conducted to assess the uncertainty of contribution associated with the reduction rates. In Isesaki and Kumagaya, uncertainty of contribution of metropolitan area was 10% to 20% and non-metropolitan was about 10%. The contribution of the non-metropolitan area is 45–70% and that of the metropolitan area is less than 10% in the morning on 22 July, when O_3 concentration was the highest in this period. In other days there are cases where the contribution from the metropolitan area was up to about 50% at Kumagaya, but the metropolitan area had a lower contribution to high O_3 concentration at Isesaki. Around these two points, 80–100 ppb O_3 is generated by 12:00 in several days of this period, during which contribution of the metropolitan area was low, and that of the non-metropolitan area was the main factor behind high O_3 concentration in the morning. After midday, the metropolitan area contribution has increased due to transport of precursors emitted from the coastal area by sea breeze. Figure 4.5(a) shows the spatial distribution of O_3 concentration predicted by the base simulation for 22 July, and Figs. 4.5(b) and (c) show the contributions of the metropolitan and non-metropolitan areas for the same day. Figure 4.5(a) shows a high O_3 concentration of about 90 ppb at 09:00 in parts of inland Kanto. The sea breeze did not extend to inland by 12:00, but O_3 concentrations had reached about 130 ppb at Isesaki and its surrounding area. Moreover O_3 concentration reached 130ppb in a part of west side of Kanto. At 09:00, precursors emitted from the metropolitan area contributed to inhibite O_3 generation in the coastal area. In inland, the contribution of the metropolitan area was low (10% or less). The contribution from non-metropolitan areas was high from 09:00 to 12:00 over almost the entirety of Kanto. The distribution of high O_3 concentration and the contribution of non-metropolitan areas were in good agreement, especially in inland Kanto. This finding indicates that, in this period, a major factor for morning high O_3 concentrations in the inland Kanto region was precursors emitted from non-metropolitan areas. After midday, sea breezes transported precursors from the coastal area to the inland, and these

precursors affected the O_3 concentration. At 15:00, contribution of the metropolitan area became greater than at 12:00 in the air mass which sea breeze transported. The contribution from the non-metropolitan area is about 60 to 80 ppb, close to the level contributied by metropolitan area on the air mass. After 15:00, the contribution from the metropolitan area decreased over the entire Kanto, and precursors from the non-metropolitan areas were a dominant factor behind the O_3 concentration.

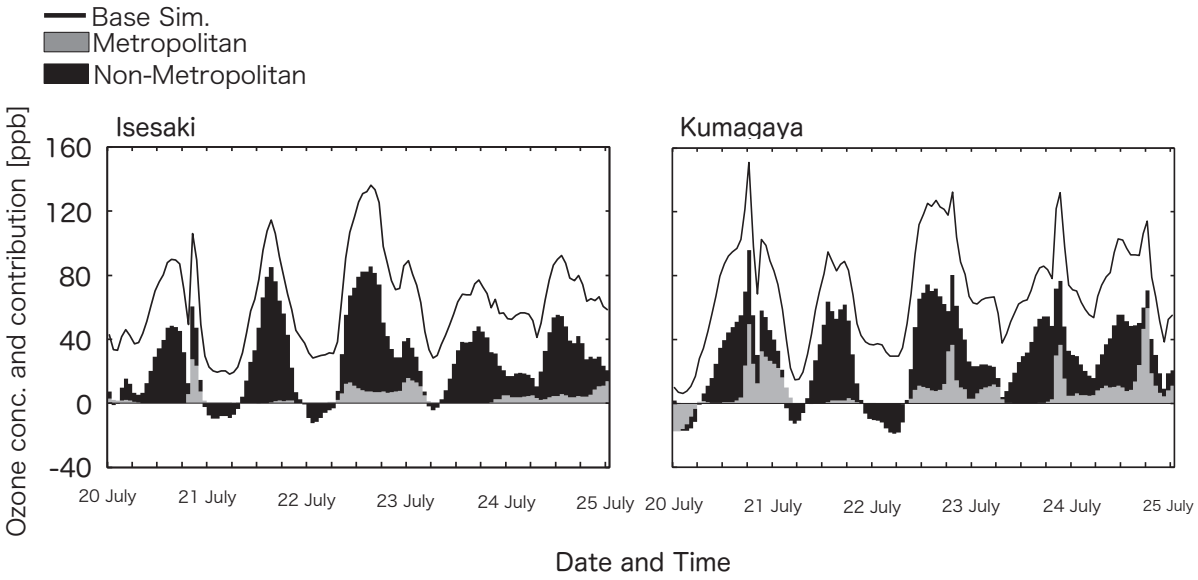

Fig.4.4 Time series of O_3 concentration in the base case simulation and contribution of metropolitan and non-metropolitan areas from 20 to 25 July at Isesaki (left) and Kumagaya (right). (This figure was derived from Kiriyama et al. accepted by Asian Journal of Atmospheric Environment)

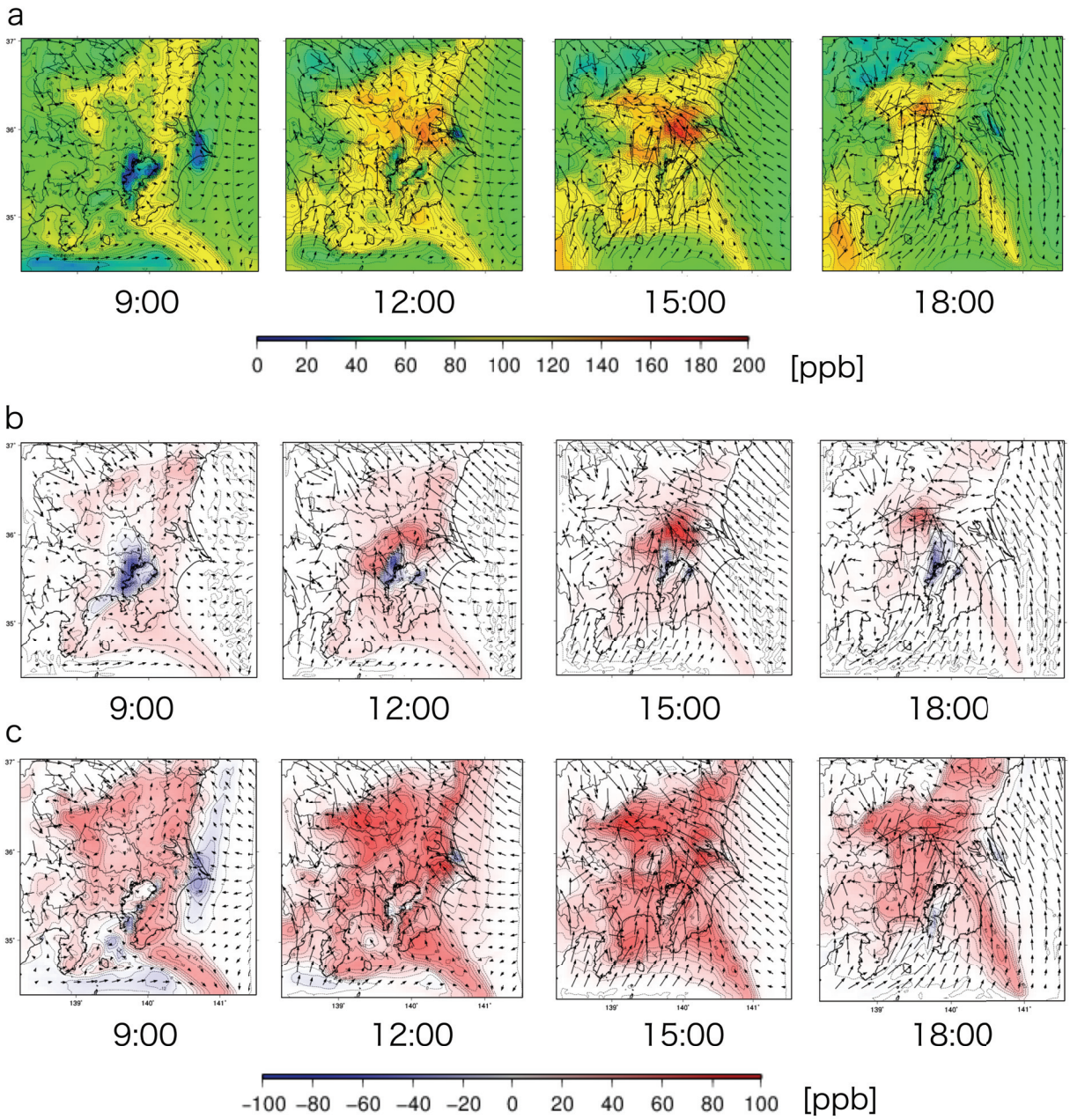

Fig. 4.5 Spatial distributions of (a) O_3 concentration and contributions of (b) metropolitan and (c) non-metropolitan areas on 22 July. (this figure was derived from Kiriyama et al. accepted by Asian Journal of Atmospheric Environment)

4.2.2 Period from 5 to 8 August

Figure 4.6 shows the same as Fig. 4.4 but from 5 to 8 August. During this period, contributions of the metropolitan and non-metropolitan area were often negative due to the titration effect due to NOx emitted from each area at nighttime and in the early morning. In the morning, the contribution of the metropolitan area accounted for around 10% at Isesaki and Kumagaya, while the contribution of the non-metropolitan area accounted for 20–67% at Isesaki and 20–50% at Kumagaya. From 20 to 24 July (the period discussed in section 4.2.1), the non-metropolitan area had a higher effect and the metropolitan areas had a lower effect on O_3 generation. Comparing from 20 to 24 July and from 5 to 8 August at Kumagaya, O_3 concentrations between 5 and 8 August were lower than that between 20 and 24 July, although the contributions of each of the areas were nearly the same. While at Isesaki, the contribution from the metropolitan area increased compared to 20 to 24 July. After midday, the sea breeze arrived at Kumagaya from 13:00 to 14:00 and at Isesaki from 15:00 to 16:00, and the contribution from metropolitan area increased at these times. Additionally, the metropolitan area had small effect on O_3 generation at Isesaki from 20 to 24 July, but during this period contributed about 20 ppb to O_3 concentration after sea breeze passage, similar as at Kumagaya. Figures 4.7 shows the same as Fig. 4.5 but for 6 August. As Fig. 4.7(a) shows, at 09:00 up to 60 ppb O_3 was distributed in some parts of the inland Kanto region. In such relatively high-concentration areas, the contribution from the metropolitan area is several ppb, but the contribution from non-metropolitan area accounts for about 50% in this area and is a major factor for O_3 concentration in the inland-Kanto region at this time. At 12:00, 70–90 ppb O_3 is distributed in the inland. Wind speeds simulated for this area were faster than at 09:00, and winds were southerly. Similar distribution patterns appeared in the O_3 concentration and the contribution from non-metropolitan area in this period. Therefore most highly O_3-polluted areas were affected by precursors from non-metropolitan areas in the same manner as on 22 July (discussed in section 4.2.1). At 15:00, precursors transported by sea breeze from the coastal area spread around Isesaki and Kumagaya, contributing to O_3. The contribution from the metropolitan area increased in comparison with 22 July, and in some locations exceeded the non-metropolitan contribution, but in many high O_3 areas there was a higher non-metropolitan contribution. At 18:00, the contribution from the metropolitan area reached similar level as the contribution from the non-metropolitan area in remote parts of the Kanto region. and O_3 distribution paralleled the contribution from the metropolitan area. The metropolitan area greatly contributed to O_3 concentration in the inland Kanto region in this period more than the period from 20 to 24 July. From Figs. 4.6 and 4.7, however, contribution from metropolitan area

did not exceed that from the non-metropolitan area at least Isesaki and the north throughout daytime. Moreover, contribution from the non-metropolitan area was greater than that of the metropolitan area in the morning. These findings indicate that during this period, too, precursors from non-metropolitan areas were a major factor behind high O_3 concentration.

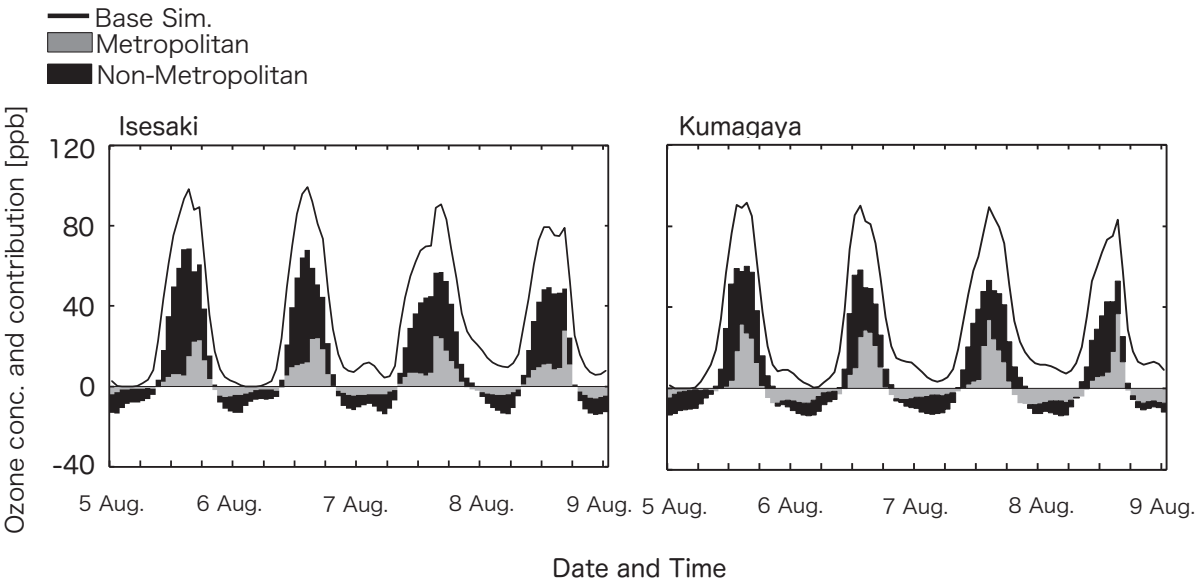

Fig. 4.6 Time series of O_3 concentration of the base case simulation and contribution of metropolitan and non-metropolitan areas at Isesaki (left) and Kumagaya (right) from 5 to 8 August. (this figure was derived from Kiriyama et al. accepted by Asian Journal of Atmospheric Environment)

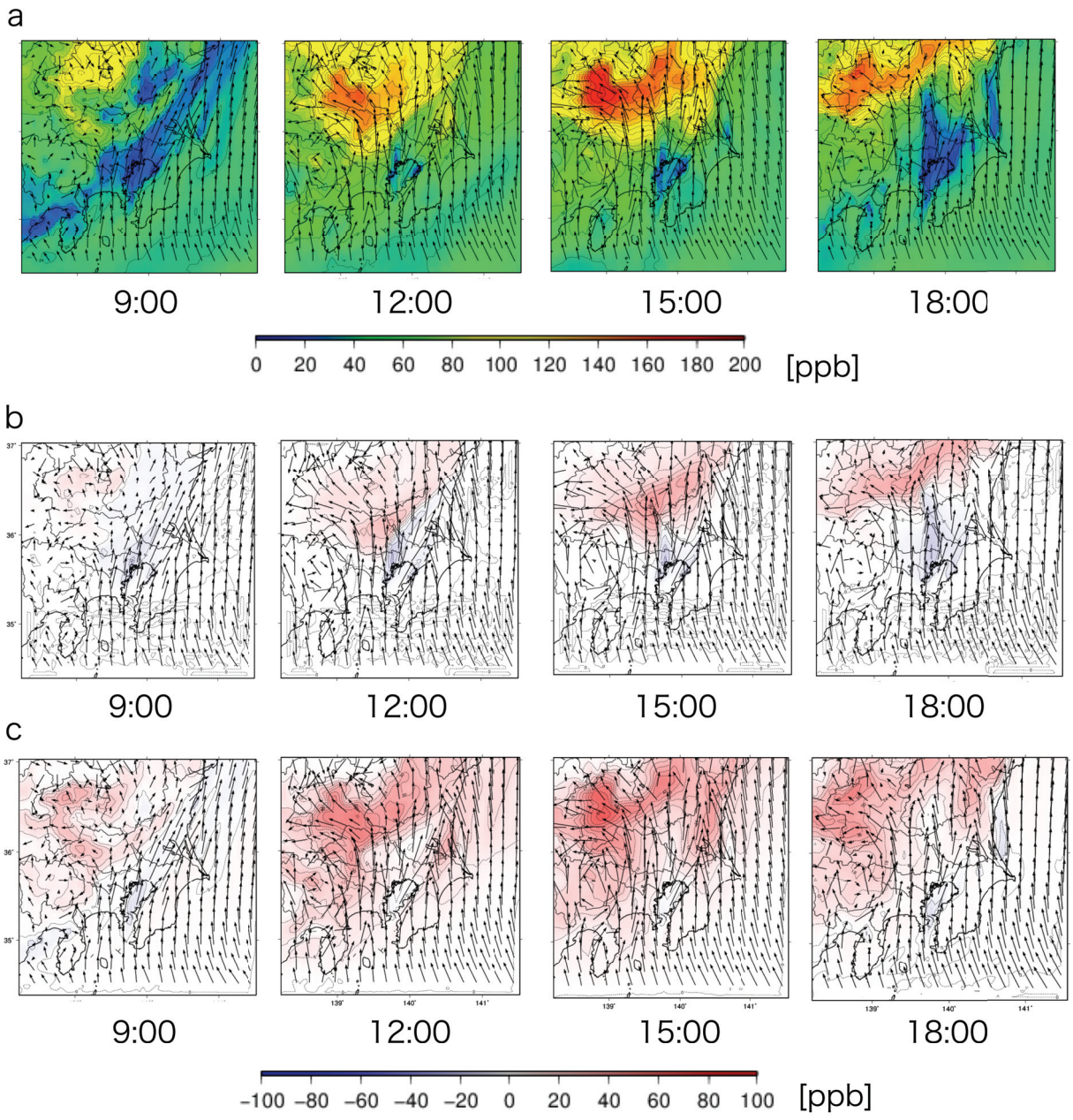

Fig. 4.7 Spatial distribution of (a) O_3 concentration and contribution of (b) metropolitan and (c) non-metropolitan areas on 6 August. (this figure was derived from Kiriyama et al. accepted by Asian Journal of Atmospheric Environment)

4.3 Relation of upper residual O_3 and morning surface O_3 concentration.

Figure 4.8 shows a time series for results of the base case and the No_chem case at Kumagaya on 22 July and 6 August. As shown in Fig. 4.8, O_3 concentration increased by 20–30 ppb although there is no chemical reaction. O_3 concentration in the No_chem case accounts for 40–80% of the base simulation by 10:00 on 20 July and 8 August, when the O_3 concentration increased by 30 ppb from the minimal morning value. This phenomenon is also seen in other days, especially on the period from 5 to 8 August discussed in the previous section. Furthermore, this phenomenon occurred not only in Kumagaya but also in Isesaki and other points of inland Kanto region, suggesting that this is not a local phenomenon. The reason for increased O_3 concentration in a non-chemical reaction environment is likely horizontal or vertical transport. As shown in Figs. 4.5 and 4.7, wind speeds in the inland were slow, and O_3 concentration was distributed uniformly at 09:00. Horizontal transportation of O_3 therefore likely has little effect on O_3 concentration, and vertical transportation of O_3 from the upper residual air to near the surface will be the main factor for increase of O_3 concentration in No_case on 22 July and 8 August. Figures 4.9(a), (b), and (c) show time–height cross sections of O_3 concentration simulated in the No_chem case, and the metropolitan and non-metropolitan contributions at Kumagaya on 22 July, respectively. Solid lines shown in Figs. 4.9(a), (b) and (c) indicate the Planetaly Boundary Layer height. As Fig. 4.9(a) shows, residual O_3 of about 80–100 ppb existed at the altitude from 550–1100 m from 05:00 to 09:00. Isopleth lines extend downward from 7:00 to 11:00, indicating entrainment of residual O_3 near the surface. During the period the surface O_3 concentration was increased by the entrainment. This phenomenon indicates that the upper residual O_3 will be another factor behind increasing O_3, increasing the importance of O_3 concentrations in the upper air during early morning. In the episode analyzed in this study, also important is that emission reduction in non-metropolitan area is more effective in this upper air O_3. As shown in Fig. 4.9(b), there was a relatively high metropolitan contribution in the upper air as compared to near the surface. Yet the contribution of the non-metropolitan area to residual O_3 was about 50 ppb, accounting for about 50% of the No_chem case result; the non-metropolitan contribution thus constitutes a large portion of O_3 entrained from the upper air.

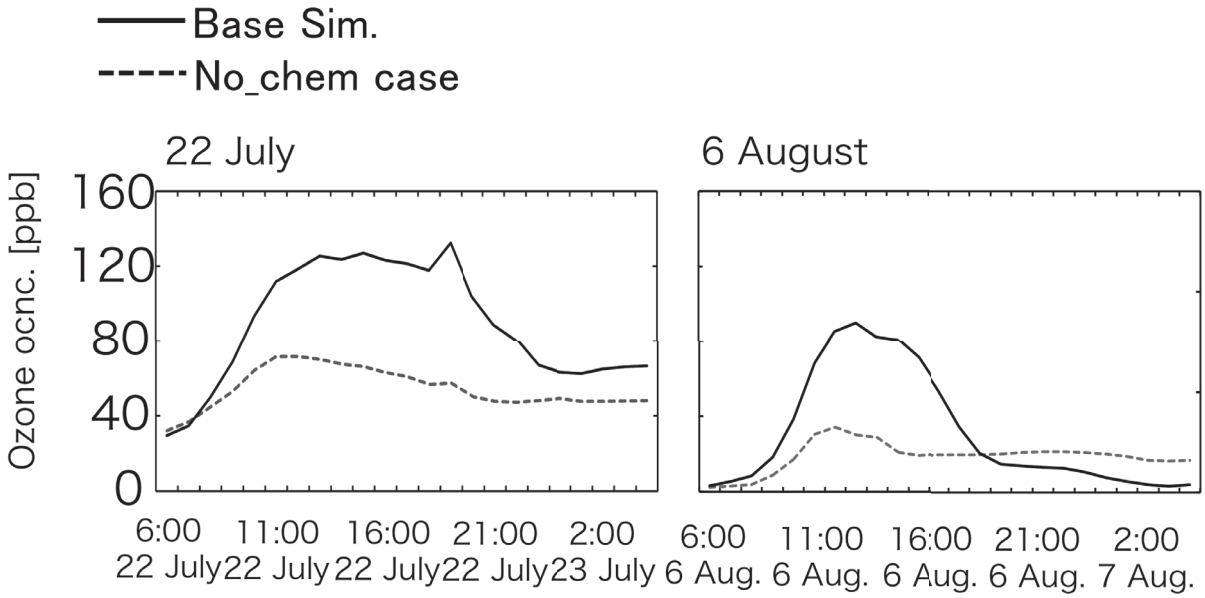

Fig. 4.8 Time series of O_3 concentration in the base case and No_chem case simulations at Kumagaya on 22 July and 6 August. Solid lines indicate base case simulation results and broken lines indicate No_chem case simulation results. (this figure was derived from Kiriyama et al. accepted by Asian Journal of Atmospheric Environment)

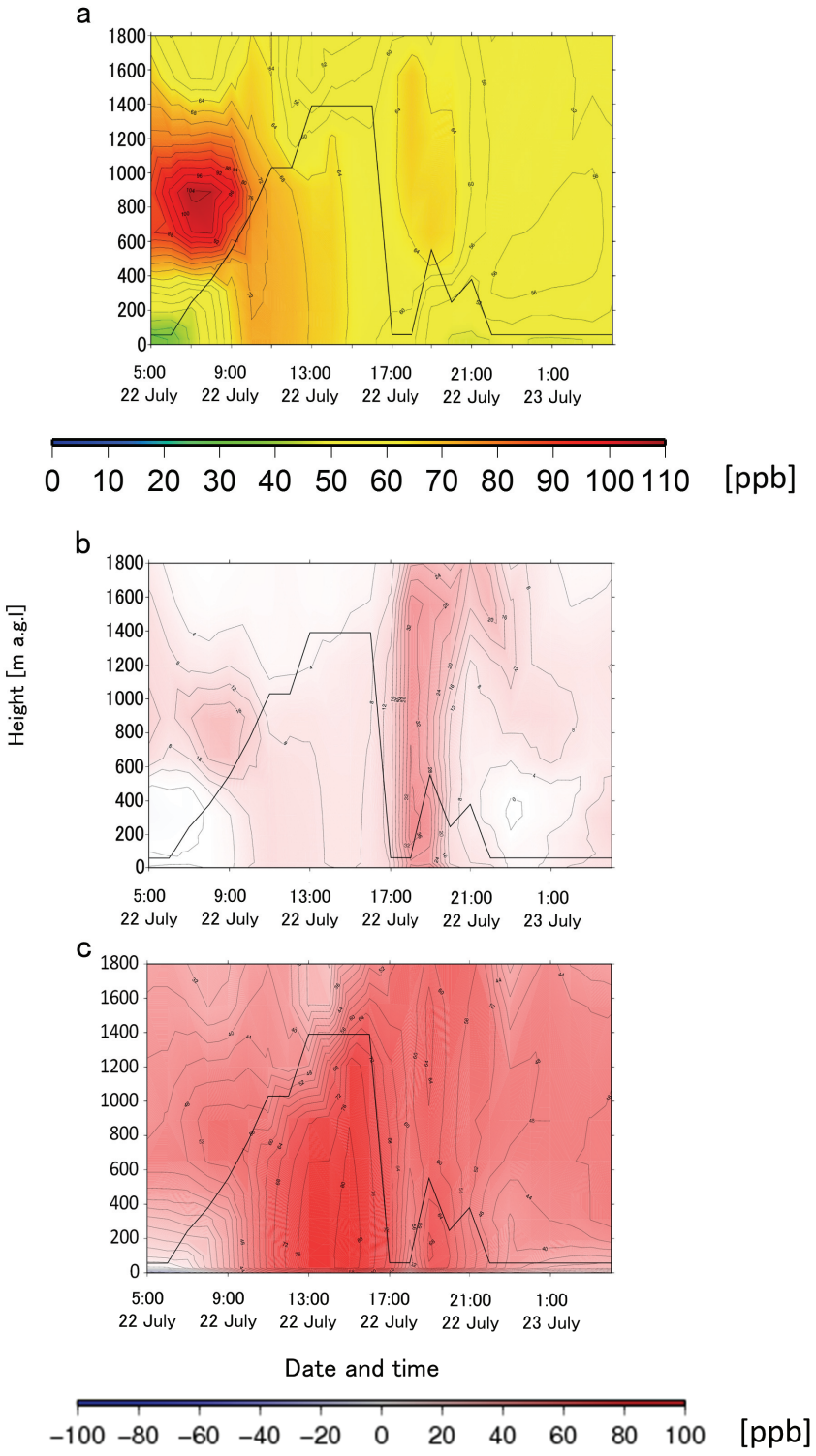

Fig. 4.9 Time–height cross-section of (a) No_chem case simulation O_3 concentrations and the contribution of (b) metropolitan and (c) non-metropolitan areas at Kumagaya from 5:00 22 to 4:00 23 July. Solid lines indicate the PBL height. (this figure was derived from Kiriyama et al. accepted by Asian Journal of Atmospheric Environment)

4.3 Conclusion of Chapter 4

To address the problem of high O_3 concentrations, especially during the morning, in the inland Kanto region of Japan, investigation of the response of O_3 concentration to emissions of O_3 precursors from the metropolitan and the non-metropolitan area was conducted by use of the WRF and the CMAQ models. Focusing on 22 July, 2010, the contribution from the metropolitan area accounted for less than 10% of the base case results. On other high O_3 concentration days in the period from 20 to 24 July, 2010, the contribution from the metropolitan area was nearly zero in the mornings, and the contribution from the non-metropolitan area accounted for 45–70%. In contrast, during the period from 5 to 8 August, 2010, both metropolitan and non-metropolitan contributions appeared throughout the day. But also during this period the non-metropolitan area significantly contributed to O_3 concentrations in the inland, with contributions of 20–60% at Isesaki and 20–50% at Kumagaya. The spatial distribution also showed that non-metropolitan areas contributed to O_3 concentrations in the inland. The example of 22 July shows that precursors from the metropolitan area had a small, narrow effect in the inland. The example of 6 August shows that sea breeze transported precursors from the metropolitan area to remote parts of Kanto and affected O_3 concentrations along the penetration path of sea breezes. Moreover, results of the No_chem case showed increase of O_3 concentrations without secondary formation. This increase results from entrainment of upper residual O_3 through the development of the planetary boundary layer. The non-metropolitan area has larger contribution to residual O_3 in the upper air than the metropolitan area.

It is indicated that the contribution of the non-metropolitan areas greatly contributed to high O_3 concentration in the inland Kanto region, especially in the morning, while the contribution of the metropolitan area was small. But as shown in Figs. 4.5 and 4.7, contributions of precursors emitted from the metropolitan area to O_3 concentration were sometimes comparable to contributions of non-metropolitan area along the path of the sea breeze. Therefore, the results of the present study will not deny the importance of transportation of precursors emitted from metropolitan area for air quality of Kanto region.

5. Conclusion

O_3 is a gas with harmful effects on living organisms, and improving O_3 air pollution is an important issue. Various emission control measures have been enacted in Japan, which have led to year-on-year decreases in the concentrations of O_3 precursors. However, O_3 concentration has tended to increase over the long term. Therefore, the effect of reducing O_3 precursors through emission control measures for the purposes of lowering O_3 concentration must be evaluated to provide more effective emission controls. In inland Kanto in the morning, a cause of the high O_3 concentration was thought to be O_3 production from O_3 precursors emitted in inland areas, but some studies have suggested other factors, which have not been explored in detail. In the present study, numerical model simulation was conducted to evaluate the effect of reduction in the emissions of O_3 precursors from 2000 to 2005 and to clarify the cause of high O_3 concentration observed in inland Kanto in the morning.

In Chapter 1, the background of O_3 air pollution was described for the introduction of this thesis. First, the general problem of O_3 air pollution and some properties of emission control measures in Japan were described. Additionally, core chemical reactions between O_3 and its precursors were summarized. Possible causes for high concentrations of O_3 in Kanto and related previous studies were described.

In Chapter 2, a summary of models and simulation conditions used in this study was shown.

In Chapter 3, the effects of reduction in anthropogenic O_3 precursors on O_3 concentration in Kanto in summer were shown. In Kanto, reductions of the emissions of anthropogenic O_3 precursors led to improved O_3 air pollution. The reduction of anthropogenic VOC emission has a strong effect on reduction of O_3 concentration in Kanto, especially in central Tokyo. However, reduction of anthropogenic NOx emissions lead to increased O_3 concentration in the coastal urban areas extending to central Saitama Prefecture. In inland Kanto, NOx emissions reductions also lead to a decrease in O_3 concentration. The reason for these different relations between O_3 and its precursors is their non-linear relationships. O_3's sensitivity to its precursors changes depending on NOx and VOC concentrations (i.e. the O_3 sensitivity regime), and the features of O_3 sensitivity regimes in Kanto were therefore also shown in this chapter. The VOC sensitive regime is dominant in the coastal area and the NOx sensitive regime is dominant in the inland for the daytime maximum of O_3 concentration of each area.

In Chapter 4, causes of the high concentration O_3 in the morning in inland Kanto were shown. Precursors emitted in the non-metropolitan area were a greater contributor to the high O_3 concentration in the morning in the inland than they

were in the metropolitan area. Entrainment of residual O_3 in the upper air due to the development of a planetary boundary layer also played an important role in the increase of O_3 concentrations inland in the morning. Even when no chemical reactions were assumed to take place, O_3 concentration was increased via mixing with upper residual O_3 in the morning. Upper residual O_3 was also contributed by precursors emitted in non-metropolitan areas. Furthermore, precursors emitted in metropolitan areas contributed in the afternoon due to the transport of O_3 and its precursors via sea breezes.

As described above, two model simulations were conducted to contribute to improvement of O_3 air pollution in Kanto in summer. For the high O_3 concentration in daytime, extending from over a single day to several days, reduction of VOC emissions was predicted to reduce the O_3 concentration by 2-5 ppb in and around central Tokyo. However, reduction of NOx emissions led to increased O_3 concentration by 1-3 ppb. As a result, NOx and VOC emisson reduction are responsible for a 2 tO_3 ppb decrease in the O_3 concentration in and around central Tokyo. In the inland Kanto region, however, this reduction of NOx emission in and around central Tokyo will likely decrease the daytime maximum O_3 concentration inland by about 2 ppb. Furthermore, the high O_3 concentration in the inland is also caused by O_3 precursors emitted in non-metropolitan areas and entrainment of the upper residual O_3. Reduction of emissions of O_3 precursors throughout the Kanto region is therefore needed to reduce daytime O_3 concentration in the region's inland areas. For the longer term, NOx and VOC emission reductions can decrease the O_3 concentration from 2 tO_3 ppb in Kanto in summer. Note that spatial distributions of increases and decreases of O_3 concentration through reductions of each O_3 precursor are similar throughout the Kanto region even if all days are set to be in summer or at high concentrations. Hence, middle- and long-term improvement of O_3 air pollution is needed to consider differences of sensitivity of O_3 to NOx and VOC for individual areas. Therefore, emission controls focused solely on the large urban area are not a fundamental solution to the problem of O_3 air pollution in Kanto, and what is instead required is cooperative emission controls in each of the region's prefectures.

Acknowledgment

I am grateful to Dr. H. Hayami and Prof. K. Miura for valuable guidance and continuous encouragements. I am also grateful to Dr. H. Shimadera for helping with using of WRF, CMAQ and involved programs and for important advice. I would like to thank Dr. S. Itahashi for many useful suggestions and discussions. I would like to thank Dr. T. Morikawa and Dr. S. Nakatsuka for providing me a precious domestic emission inventories.

I am grateful to National Institute for Environmental Study for providing me long-term O_3 monitoring data. I am also grateful to Generic Mapping Tools (GMT) developers for providing me a useful mapping tool to making various maps and vertical distributions.

References

Byun, D. W., Ching, J.: Science algorithms of the EPA Models-3 Community Multiscale Air Quality (CMAQ) modeling System. EPA/600/R-99/030 (1999)

Byun, D. W., Schere, K.L.: Review of the governing equations, computational algorithms, and other components of the Models-3 Community Multiscale Air Quality (CMAQ) modelling system. *Appl. Mech. Rev.*, 59, 51-77 (2006)

Carter, W. P. L.: Implementation of the SAPRC-99 Chemical Mechanism into the Models-3 Framework, Report to the United States Environmental Protection Agency. (2000)

Chen F., Dudhia J. (2001) Coupling an advanced land-surface/ hydrology model with the Penn State/NCAR MM5 modeling system - Part I: Model implementation and sensitivity. *Monthly Weather Review*, 129(4), 569-585.

Emmons, L. K., Walters, S., Hess, P. G., Lamarque, J.-F., Pfister, G. G., Fillmore, D., Granier, C., Guenther, A., Kinnison, D., Laepple, T., Orlando, J., Tie, X. Tyndall, G., Wiedinmyer, C., Baugghcum, S. L., Kloster, S. (2010) Description and evaluation of the Model for Ozone and Related chemical Tracers, version 4 (MOZART-4). *Geosci. Model Dev.*, 3, 43-67.

Gégo, E., Gilliland, A., Godowitch, J., Rao, S. T., Porter, P. S., Hogrefe, C.: Modeling Analyses of the Effects of Changes in Nitrogen Oxides Emissions from the Electric Power Sector on Ozone Levels in the Eastern United States. *Air & Waste Manage. Assoc.*, 58, 580–588, (2008)

Guenther, A., Karl, T., Harley, P., Wiedinmyer, C., Palmer, P.I., Geron, C.: Estimates of global terrestrial isoprene emissions using MEGAN (Model of Emissions of Gases and Aerosols from Nature). *Atmos. Chem. Phys.*, 6, 3181-3210 (2006)

Hong, S.-Y., Lim, J.-O.J.: The WRF Single-Moment 6-Class Microphysics Scheme (WSM6). *J. Korean Meteor. Soc.*, 42, 129-151 (2006)

Hong, S–Y, Noh, Y, Dudhia, J.: A new vertical diffusion package with an explicit treatment of entrainment processes. *Mon. Wea. Rev.*, 134, 2318–2341 (2006)

Hosoi, S., Yoshikado, H., Sekiguchi, K, Wang, Q., Sakamoto, K. (2011) Daytime meteorological structures causing elevated photochemical oxidants concentrations in north Kanto, Japan. A*tmos. Environ.*, 45, 4421-4428.

Iacono, M. J., Delamere, J. S., Mlawer, E. J., Shephard, M. W., Clough, S. A., Collins, W. D.: Radiative forcing by

long–lived greenhouse gases: Calculations with the AER radiative transfer models. *J. Geophys. Res.*, 113, D13103, doi:10.1029/2008JD009944 (2008)

Inoue, K., Yasuda, R., Yoshikado, H., Higashino, H.: Spatial distribution of summer-time surface ozone sensitivity to NOx and VOC emissions for the Kanto area Part 1:Estimasion by numerical simulations with two kinds of (lager and smaller) biogenic emission estimates. J. *Jpn. Soc. Atmos. Environ.*, 45, 5, 183-194 (2010) [in Japanese with English abstract and figure captions]

Jacob, D. J.: Introduction to Atmospheric Chemistry, pp.234-239, *Princeton University Press, New Jersey* (1999)

Janjic, Z. I.: Nonsingular Implementation of the Mellor-Yamada Level 2.5 Scheme in the NCEP Meso model. NCEP Office Note, No. 437, 61 pp (2002)

Kain, J.S.: The Kain-Fritsch convective parameterization: An update. *J. Appl. Meteorol.*, 43, 170-181 (2004)

Kiriyama, Y., Hayami, H., Awasaki, T., Miura, K., Kumagai, K., Yamaguchi, N.: Influence of development of mixing layer for ozone concentration in inland Kanto area in summertime. *J. Jpn. Soc. Atmos. Environ.*, 47, 81-86 (2012) [in Japanese with English abstract and figure caption]

Kiriyama, Y., Shimadera, H., Itahash, S., Hayami, H., Miura., K.: Evaluation of the effect of regional pollutants and residual ozone on ozone concentrations in the morning in the inland of the Kanto region. *Asian J. Atmos. Environ*., (now printing)

Kiriyama, Y., Hayami, H., Itahashi, S., Shimadera, H., Miura, K., Nakatsuka, S., Morikawa, T.: Effect of NOx and VOC controls for surface ozone concentration in summertime in Kanto region of Japan. *J. Jpn. Soc. Atmos. Environ.*, (in press)

Kurita, H., Sasaki, K., Muroga, H., Ueda, H., Wakamatsu, S.: Long-Range Transport of Air Pollution under Light Gradient Wind Conditions. *J. Clim. Appel. Meteorol.*, 24, 425-434 (1985)

Laprise, R.: The Euler equations of motion with hydrostatic pressure as an independent variable. *Mon. Wea. Rev.,* 120, 197– 207 (1992)

Ministry of Education: Dynamics of air pollution in the inland region, "Environmental Science" report, Ministry of Education, Tokyo, Japan, B280-R11-2 (1986)

Ministry of Environment, Japan (MOE): *Survey report for photochemical air pollution*., 1-174, (2012)

Ministry of Environment, Japan (MOE): *Survey report for photochemical air pollution.*, 1-174, (2014)

Morikawa, T., Chatani, S., Nakatsuka, S.: Technical report of the Japan Auto-Oil program: Estimate of emissions from vehicles. Rep. JPEC-2011 AQ-02-06, Japan Petroleum Energy Center, Minato-ku, Japan. (2012) [in Japanese]

Muramatsu, H.: A Case Study of the Transport of the Stratospheric Ozone into the Troposphere. *Pap. Met. Geophys.*, 31, 97-105 (1980)

Nagashima, T., Ohara, T., Sudo, K., Akimoto, H.: The relative importance of various source regions on East Asian surface ozone. *Atmos. Chem. Phys.*, 10, 11305-11322 (2010)

Nakatsuka, S., Morikawa, T., Chatani, S., Matsunaga, S. Technical report of the Japan Auto-Oil program: Estimate of emissions from sectors other than vehicles. Rep. JPEC-2011 AQ-02-07, Japan Petroleum Energy Center, Minato-ku, Japan. (2012) [in Japanese]

Nawahada, A., Yamashita, K., Ohara, T., Kurokawa, J., Yamaji, K.: Evaluation of Premature Mortality Caused by Exposure to $PM_{2.5}$ and Ozone in East Asia: 2000, 2005, 2020. *Water Air Soil Pollut.*, 223, 3445-3459 (2012)

Niwano, M., Takigawa, M., Takahashi, M., Akimoto, H., Nakazato, M., Nagai, T., Sakai, T., Mano, Y.: Evaluation of Vertical Ozone Profiles Simulated by WRF/Chem Using Lidar-Observed Data. *SOLA*, 3, 133-136 (2007)

Ohara T., Akimoto H., Kurokawa J., Horii N., Yamaji K., Yan X., Hayasaka T.: An Asian emission inventory of anthropogenic emission sources for the period 1980-2020. *Atmos. Chem. Phys.*, 7, 4419-4444 (2007)

OPRF : Report on the Project for Estimating the Impact of Designation of Emission Control Area on Improvements in Air Quality. Rep. ISBN978-4-88404-282-0, Minato-ku, Tokyo, Japan. (2012) [in Japanese]

Pochanart, P., Akimoto, H., Kinjo, Y., Tanimoto, H.: Surface ozone at four remote island sites and the preliminary assessment of the exceedances of its critical level in Japan. *Atmos. Environ.*, 36, 4235-4250 (2002)

Reynolds, R.E., Smith, T.M., Liu, C., Chelto, D.B., Casey K.S., Cchlax M.G.: Daily High-Resolution-BlendedAnalysis for Sea Surface Temperature. *J. Climate.* 20, 5473-5495 (2007)

Seinfeld, J. H., Pandis, S. N.: Atmospheric Chemistry and Physics. 2nd. Ed. pp.239-241, 1182-1185, *Jhon Wiley & Sons, Inc., New Jersey* (2006)

Sillman, S., He, D., Pippin, M. R., Daum, P. H., Imre, D. G., Kleinman, L. I., Lee, J. H., Weinstein-Lloyd, J.: Model correlations for ozone, reactive nitrogen, and preoxides for Nashville in comparison with measurements: Implications for O_3-NOx-hydrocarbon chemistry. *J. Geophys. Res.* 103 (D17), 22629-22644 (1998)

Sillman, S., He, D.: Some theoretical results concerning O_3-NOx-VOC chemistry and NOx-VOC indicators. *J. Geophys.*

Res. 107, doi:10.1029/2001JD001123 (2002)

Skamarock W.C., Klemp J.B., Dudhia J., Gill D.O., Baker, D.M., Duda, M.G., Huang, X.-Y., Wang, W., Powers, J.G.: A description of the advanced research WRF version 3. NCAR Technical Note, NCAR/TN-475+STR (2008)

Skamarock, W.C., Klemp, J.B.: A time-split nonhydrostatic atmospheric model for weather research and forecasting applications. *J. Comput. Phys.*, 227, 3465-3485 (2008)

US Environmental Protection Agency: Air Quality Criteria for Ozone and Related Photochemical Oxidants (Final), US Environmental Protection Agency, Washington, DC, USA, EPA/600/R-05/004aF-cF (2006).

Wakamatsu, S., Ogawa, Y., Murano, K., Goi, K., Aburamoto, Y.: Aircraft survey of the secondary photochemical pollutants covering the Tokyo metropolitan area. *Atmos. Environ.*, 17, 827-835 (1983)

Wakamatsu, S., Morikawa, T., Ito, A.: Air Pollution Trends in Japan between 1970 and 2012 and Impact of Urban Air Pollution Countermeasures. *Asian J. Atmos. Environ.*, 7, 177-190 (2013)

Wang, H., Kiang, C. S., Xiaoyan, T., Xiuji, Z., and Chameides, W. L.: Surface ozone: A likely threat to crops in Yangtze delta of China. *Atmos. Environ.*, 39, 3843-3850 (2005)

Yoshikado, H.: Air Pollution in Japan Dominated by Local Meteorology. *J. Jpn. Soc. Atmos. Environ.*, 42, 63-74 (2007) [in Japanese with English abstract and figure captions]

Zhang, Q., Streets, D. G., Carmichael, G. R., He, K., Huo, H., Kannnari, A., Klimont, Z., Park, I., Reddy, S., Fu, J. S., Chen, D., Duan, L., Lei, Y., Wang, L., Yao, Z.: Asian emissions in 2006 for the NASA INTEX-B mission. *Atmos. Chem. Phys.*, 9, 5131-5153 (2009)